V-ATPASE AT THE CELL SURFACE IN HIGHLY METASTATIC PROSTATE CANCER CELLS

by

LUIS E. BERMUDEZ, B.S.

A THESIS

IN

PHYSIOLOGY

Submitted to the Graduate Faculty of
Texas Tech University Health Sciences Center
in Partial Fulfillment of the Requirements
for the Degree of

MASTER OF SCIENCE

Advisory Committee

Raul Martinez-Zaguilán (Chairperson)
Stephanie Filleur
Jose F. Perez-Zoghbi

Accepted

Thomas A. Pressley, Ph.D.
Interim Dean of the Graduate School of Biomedical Sciences
Texas Tech University Health Sciences Center

December 2010

ACKNOWLEDGEMENTS

The work I have completed here could not have been possible without the help of my family, my friends and my co-workers. I dedicate this work to the two people who not only gave me the encouragement to pursue my dreams but also provided all the economic and emotional support. My father Carlos Eduardo Bermudez and my mother Yubelly Rojas, both of them are successful physicians and successful parents. Both of them managed what many people could not, to have an accomplished professional life and a loving family. Equally, both are my source of inspiration and my goal.

I was very fortunate to work in a lab where each member is always ready to help each other. I want to thank Jood Hashem and Jess Lees for working with me all the late nights. Thanks to them I was able to keep pushing when the science did not cooperate. Dr. Souad Sennoune was the keystone in the advancement of my project. Since the first day I started working in this lab, she was patient and taught me the procedures I needed to complete my project. She taught me by pointing me in the right direction and not giving me the answers. All the knowledge and wisdom that she provided made me a better scientist and a better person.

My mentor and friend Dr. Raul Martinez-Zaguilan is responsible not only for the level of understanding necessary for this project, but also for nurturing my curiosity and critical thinking skills. Thanks to him I enjoyed the process of developing a working hypothesis and working hard to test it. I am proud to call him my mentor and I hope that he is proud of helping me complete this goal. I also want to thank the members of my committee (Drs. Jose

Perez-Zoghbi and Stephanie Filleur) for their assistance, patience and guidance. I would like to specially thank Stephanie for providing me with the cell lines necessary for this project and for allowing me to use her equipment to test some of my hypotheses. Finally, I would like to thank Dr. Lan Guan and Dr. Luis Cuello, and the members of their labs for all the help and guidance that they provided.

TABLE OF CONTENTS

Texas Tech University Health Science Center, Luis E. Bermudez, December 2010

ABSTRACT

Prostatic adenocarcinoma is the second-leading cause of cancer death of men in the United States. The threat comes from the cancer metastasizing to distant organs. Metastatic tumors are highly glycolytic in nature and they tend to undergo anaerobic metabolism. This leads to the production of lactic acid that could result in intracellular acidosis. To survive in this environment, cells regulate their pH by expressing several transporters. We hypothesize that metastatic prostate cancer cells use plasma membrane Vacuolar H^+-ATPases (pm-V-ATPases) to counteract intracellular acidosis. V-ATPases are typically found in intracellular acidic compartments. It has been previously shown that V-ATPases at the cell surface are involved in breast cancer metastasis, invasiveness, and drug resistance. It has also been previously shown that isoforms of the *a* subunit of the V-ATPase targets the cell to the cell surface. In this study, we show that V-ATPases are localized at the cell surface in highly metastatic prostate cancer cells using immunocytochemistry. We show that the mRNA levels of the *a* isoform that targets the V-ATPase to the cell surface are increased in highly metastatic prostate cancer cells. The proton fluxes and the specific activity of pmV-ATPase were also increased in highly metastatic prostate cancer cells. We show that inhibiting the V-ATPase enhances chemosensitivity in metastatic prostate cancer cells. These data indicate that V-ATPases at the cell surface are present in highly but not poorly metastatic cells. This suggests that the V-ATPase is a novel molecular target to enhance the efficacy of chemotherapeutic drugs to alleviate the consequences of prostate cancer metastasis.

LIST OF FIGURES

ABBREVIATIONS

- *ABC*: ATP Binding Cassette
- *AE:* Anion Exchanger
- *ANOVA*: Analysis of Variance
- *ATP*: Adenosine Triphosphate
- *BSA*: Bovine Serum Albumin
- *cDNA*: Complementary Deoxy Ribonucleic acid
- *CSB*: Cell Suspension Buffer
- *EDTA*: Ethylenediaminetetraacetic acid
- *HEPES*: 4-(2-hydroxyethyl)-1-piperazineethanesulfonic acid
- *HRPC*: Hormone Refractory Prostate Cancer
- IC_{50}: Half maximal inhibitory concentration
- *ICCB*: Intensity Correlation Coefficient-Based analysis
- J_{H+}: Proton Flux
- *MCT:* Monocarboxylate Transporter
- *MES*: 2-(N-morpholino)ethanesulfonic acid
- *m*RNA: Messenger Ribonucleic acid
- *NBC:* Sodium Bicarbonate Cotransporter
- *NHE*: Sodium-Proton Exchanger
- *PBS:* Phosphate Buffered Saline

- pH_i: Intracellular pH
- *PM*: Plasma Membrane
- *pmV-ATPase*: Plasma membrane Vacuolar H^+ ATPase
- *QRT-PCR*: Quantitative Reverse Transcription – Polymerase Chain Reaction
- *rRNA*: Ribosomal Ribonucleic acid
- *SDS*: Sodium Dodecyl sulfate
- *SNARF*-1: 5-[and-6] carboxy-seminaphtorhodafluor-1-acetoxymethylester

CHAPTER I

INTRODUCTION

pH Regulation in Tumors

Uncontrolled cell growth and increased metabolic activity have become hallmarks of the tumor phenotype. The abnormal glucose metabolism along with the poor perfusion due to poor vascularization causes the tumor cells to rely on glycolysis for energy (1). This produces high levels of lactic acid which could reduce the intracellular pH (pH_i). In order to control the intracellular pH, the cells use different proton transporters including the Na^+/H^+ exchanger (NHE), the proton linked monocarboxylate transporter (MCTs), the HCO_3^- based transporting mechanisms, carbonic anhydrases, and the Vacuolar type H^+-ATPase (herein referred as V -ATPase) (1).

The sodium proton exchanger (NHE) is an integral membrane protein which regulates pH by removing protons from the cytosol in exchange for extracellular sodium ion with a stoichiometry of 1:1 (2). It is ubiquitously expressed and also serves as a major sodium entry pathway. The NHE is also volume and osmolarity-sensitive and helps control the cell volume even though the mechanism is not well understood (3). The NHE is involved in cellular growth and proliferation through initiating shifts in pH_i (4). There are 9 members of the NHE family of which NHE1 is ubiquitously expressed in mammalian tissues (5). Cell proliferation is associated with the expression of NHE1. NHE1 deficient cells have been shown to either lose or severely reduce the cancer's capacity for tumor growth. However, the mechanism for proliferation regulated by the NHE1 remains unclear (6).

Bicarbonate transport through the membrane is highly important for the regulation of pH as part of the CO_2 metabolism. Carbonic anhydrase catalyzes the reaction:

$$CO_2 + H_2O \xrightarrow{\text{Carbonic anhydrase}} HCO_3^- + H^+$$

In the cell, CO_2 is a byproduct of the electron transport chain when creating ATP. Since CO_2 has poor solubility, most of it is carried in the form of HCO_3^-. Bicarbonate cannot move freely through the membrane, therefore without a protein transporter the pH_i of the cell would decrease continuously. The two main types of bicarbonate transporters are the Cl^-/HCO_3^- exchangers and the Na^+/HCO_3^- cotransporters (7,8).

The Cl^-/HCO_3^- exchangers belong to the Anion Exchanger family (AE). The AE move bicarbonate and chloride in opposite directions across the membrane. There are four AE isoforms expressed in different mammalian tissues (9,10). The Na^+/HCO_3^- cotransporters belong to the sodium bicarbonate cotransporter family (NBC). The NBC move sodium and bicarbonate together across the plasma membrane. There are four main NBC isoforms. Unlike the AE family, the NBC family isoforms can have varying stoichiometry making some isoforms electrogenic (11,12). These transporters have not been extensively studied in tumors. In renal cancer however, the von Hippel-Lindau tumor suppressor has been shown to regulate the activity of both the AE and NHE (13).

Proton linked monocarboxylate transporters (MCTs) play a major role in the cell metabolism by catalyzing the facilitated diffusion of lactate and other monocarboxylates through the plasma membrane or the mitochondria. Along with cancer cells, red blood cells and white skeletal muscle cells produce high levels of lactic acid through glycolysis. All cells however use glycolysis during hypoxia or ischemia. Without regulation of pH during an increase in lactic acid production, an acidic pH will inhibit phosphofructokinase, an essential protein in glycolysis (14). Lactic acid is also oxidized and used as respiratory fuel under certain conditions in the brain, liver, heart and red skeletal muscle. In these cases the MCTs will catalyze the influx of lactic acid (15). MCTs have 8 different isoforms that have different expression in human tissues. MCT1 is ubiquitously expressed and can transport acetate and protons. In this study we will use acetate to induce cytosolic acidification (16).

V-ATPase

The mechanism of action and structure of the V-ATPase is very similar to that of the ATP-synthase. A glance into the ATP-synthase can help us to understand the mechanism of action behind the V-ATPase. The F_0/F_1 ATP synthase is located on the inner membrane of all mitochondria and it uses the proton gradient generated by the electron transport chain to catalyze the synthesis of ATP from ADP and inorganic phosphate. ATP synthase is composed of two opposing rotary motors designated F_1 and F_0. F_0 is membrane embedded and is involved in proton translocation. F_1 is water soluble and is involved in ATP synthesis (17).

The F_0 rotor is composed of 10 to 15 c subunits arranged in a ring which span the membrane. They are connected to the *a* subunit which also spans the membrane and is involved in ion translocation through the c ring. The c ring is connected to the F1 rotor through the central stalk which is composed of subunits γ and ε. Torque generated by the movement of protons causes the central stalk to do a conformational change on the F1 rotor driving ATP synthesis. The F1 rotor is composed of 3 copies of α and β subunits in alternating arrangement. The nucleotide binding site is located on the β subunits and each αβ pair is in a different conformation which changes sequentially as the motor rotates. The rotation of the F0 rotor is counterclockwise causing the γ stalk to cause a conformational on the αβ pairs every 120° (18,19,20).

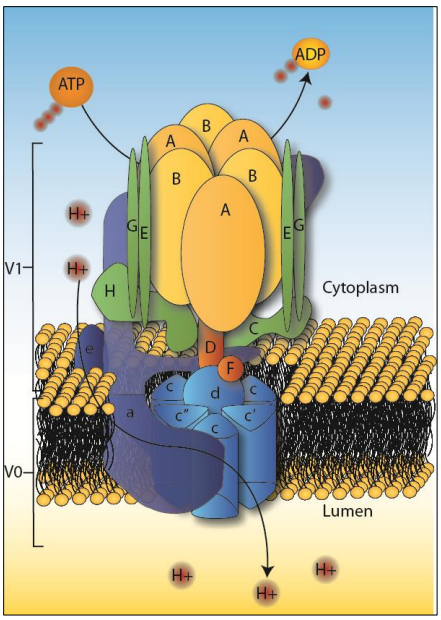

Figure 1: V-ATPase structure and function. The V-ATPase is composed of 2 domains V0 embedded in the membrane and V1 facing the cytoplasm. The V-ATPase couples the hydrolysis of ATP to the movement of protons from the cytoplasm into the lumen of acidic vesicles or outside the cell (plasma membrane V-ATPase).

The vacuolar H^+-ATPase (V-ATPase) controls the pH of intracellular organelles which serve to regulate several biological processes, including membrane trafficking, protein degradation and coupled transport of small molecules. More specific functions include renal acidification, bone resorption, and sperm maturation. The V-ATPase is composed of 14 different subunits organized into 2 domains: the ATP-hydrolytic domain (V1) and the proton-translocation domain (V0). The mechanism of V-ATPase is very similar to that of ATP synthase (F-type) in which it is a rotatory mechanism. However, unlike ATP synthase which uses an H^+ gradient to form ATP, V-ATPase uses ATP to move H^+ against its concentration gradient (21).

The V1 domains contain eight different subunits numbered A through H. Subunits A and B form the main rotor and are present in triplicates and are present in alternating arrangement. The interface between the A and B subunits constitute the ATP catalytic site, however most of the ATP binding sites are located on the A subunit. The B subunit contains nucleotide binding sites which provide a modulatory role (22). Subunits C through H constitute the central and

peripheral stalk. The central stalk couples the energy from ATP hydrolysis to the rotation mechanism on the V0 domain. The peripheral stalk serves as a stator preventing the rotation of the rotor head (21).

The V0 domain contains six different subunits numbered *a, d, e, c, c"* and Ac45. The proton transporter is composed of four to five copies of subunit c arranged in a ring. The subunits *c* and *c"* are proteolipids and are highly hydrophobic. These subunits contain a Glutamate residue which can be reversibly protonated (23). The *a* subunit is crucial for the carrying of protons across the membrane. It contains a hemi-channel facing the cytoplasmic side of the membrane and allows for the movement of protons towards the Glutamate residue in the *c* ring. Once the protons complete a full revolution around the *c* ring, an Arginine residue in the *a* subunit retrieves the proton from the *c* subunit and releases it towards the luminal side of the membrane (24). Subunit *d* is located at the top of the *c* ring and provides a connection with the central stalk of the V1 domain. Finally subunit *e* is a highly hydrophobic polypeptide found next to the *a* subunit embedded on the plasma membrane. Bafilomycin and concanamycin are specific inhibitors of the V-ATPase that bind to the *c* subunit of the V0 domain preventing rotation of helices relative to one another within the subunit. This causes the *c* ring to come to a stop and therefore prevent the movement of protons (25).

In addition to having a crucial role in the translocation of protons across the plasma membrane, subunit *a* is also involved in targeting the V-ATPase to different cellular destinations. There are 4 different isoforms numbered *a1* through *a4*. The *a1* isoform is ubiquitously expressed and is associated with the targeting of the V-ATPase to the endosomes and lysosomes (22). In renal intercalated cells and epididymal clear cells it has been shown that the isoform *a2* targets the V-ATPase to the apical endosomes while the *a4* subunit targets the V-ATPase to the apical membrane (26). In osteoclasts it has been shown that the *a3* isoform is present in both lysosomes and the plasma membrane suggesting that there is translocation of the V-ATPase upon activation of the cell (27). It has been shown in breast cancer cell lines that different expression of the *a* isoforms are present between highly and poorly metastatic cells. The breast cancer cell line MB231 is considered highly metastatic and has shown to have

high levels of mRNA encoding for isoform *a3* and *a4* compared to the poorly metastatic MCF7 cell line (28).

The V-ATPase has an active role in the progression of the tumor towards metastasis. Plasma membrane V-ATPase has been shown to acidify the environment of several tumor cell lines including breast cancer and melanoma (29). Cathepsins are proteases shown to be secreted from lysosomes in a variety of cancer cells which require an acidic environment to be functional. Activated cathepsins have the ability to degrade the extracellular matrix and activate metalloproteases which can also help in the degradation of the extracellular matrix. Without the extracellular matrix, it is easier for tumor cells to separate from the main tumor and move through the blood to distant organs (30,31). Consequently, the pmV-ATPase can help with the activation of proteases by acidifying the extracellular environment. Also, the V-ATPase can help in the trafficking of proteases from lysosomes to the extracellular matrix through increased vesicular recycling.

Multidrug Resistance

One of the biggest obstacles in effective cancer therapy is the ability of the tumor to progressively become resistant to the treatment. Cancer cells can become resistant to drugs by either blocking the absorption of the drug or by excreting the drug at increased rates. The cell can also activate detoxifying systems which repair DNA damage caused by the drug, these usually include cytochrome P450. The cell may also counteract the effects of apoptotic drugs by altering the signaling pathway; these usually involve a defective p53 or altered ceramide levels. Once the cell gains resistance to one type of drug, it becomes resistant to similar drugs creating what is known as multidrug resistance (32).

Most commonly, the multidrug resistance phenotype is a direct result of an expression of different ABC (ATP binding cassette) transporters. ABC transporters are ATP driven efflux pumps with broad drug specificity ranging from vinca alkaloids to anthracyclines and the more commonly used microtubule-stabilizing drug paclitaxel (33). In prostate cancer, the ABC transporter involved in multidrug resistance has been found to be MRP4. This transporter

usually only moves nucleotide analogues and organic anions but during multidrug resistance they have the ability to extrude the chemotherapeutic drugs methotrexate and thiopurines (34). It has been previously shown that breast cancer cell lines respond to several anticancer drugs by moving them into acidic vesicles where they become inactive. The cell then proceeds to increase the rate of vesicle recycling, extruding the inactive drug from the cell. The V-ATPase is closely involved in this process and has been suggested as a novel chemotherapeutic target (35,36).

Prostate Cancer

Prostatic adenocarcinoma is the most common cancer in men in the United States accounting for 1 in 4 of every newly diagnosed cancer. According to the American Cancer Society, it estimated that in 2010, there will be 217,730 new diagnosed cases and that 32,050 men will die from it. They estimate that 1 in 6 men in the United States will be diagnosed and 1 in 36 men will die from the disease (37). The cause and progression of prostate cancer is poorly understood, but there are risk factors that can help with early detection. Age is the most important risk factor, followed by ethnicity and family history. Men over the age of 70 have the highest incidence of the disease at 888.6 cases per 100,000 for white men and 1279.1 cases per 100,000 for African American men. Not only are African American men more likely to develop the disease, but they are also more likely to die from it. The mortality rate for white men between the years 2004-2006 in the US was 231.9 per 100,000, while for African American men was 56.3 per 100,000 (38).

Even though its presence is undeniable, the major threat is in its progression towards metastasis. When the tumor is detected at a local stage (i.e. not spread into other organs), the five-year survival rate is 100%. However, when the tumor metastasizes, the five-year survival rate decreases to 30.6% (39). Not all tumors progress at the same rate, while some progress quickly leading to premature death, some neoplasms progress slowly allowing for long-term survival. The clinical uncertainty and complexity of prostate cancer make the understanding of the metastatic phenotype an imperative concern towards the development of more effective treatments (40).

Currently there are several options for the treatment of prostate cancer. These include surgery, radiation therapy, hormone therapy and chemotherapy. Among the more common treatments include the radical prostectomy is a surgical option in which the prostate is removed and it is done before there are signs of cancer cells on the adjacent lymph nodes. Radiation therapy uses either an external source of radiation (such as x-rays) or radioactive substances which are introduced directly to the cancer in order to kill it. Chemotherapeutical approaches use mixtures of different drugs that kills rapidly growing cells by inducing apoptosis, stop the cell from dividing or damaging the DNA. Androgen deprivation prevents prostate cancer cells from growing. This is achieved through hormone therapy. Among the treatments used is the luteinizing hormone-releasing hormone agonist which prevents the testicles from releasing testosterone. This works by decreasing the pulsatility of the LH/FSH release thereby decreasing testosterone. Orchiectomy is a surgical option to remove the testicles and drastically decrease the production of testosterone (41).

Unfortunately, one of the most aggressive forms of prostate cancer occurs after hormone therapy fails to stop tumor growth, these new cancer cells have now become androgen independent. Hormone refractory prostate cancer (HRPC) typically manifests disease progression within 12 to 18 months. Currently there is no cure for HRPC and there is only a single approved treatment. The treatment involves the use of the chemotherapeutic drug docetaxel combined with prednisone or mitoxantrone. Unfortunately this only extends the median survival 16 to 18 months (42,43,44,45).

Docetaxel along with paclitaxel belong to the chemotherapeutic family of taxanes. Docetaxel and paclitaxel are derived naturally from the European yew tree and the pacific yew tree respectively. Taxotere is the commercial name for docetaxel. Docetaxel blocks the cell-cycle progression during mitosis by binding to the β-subunit of tubulin stabilizing the microtubule structure and preventing depolymerisation. This affects the cell's microtubule dynamics which are most active during mitosis. Blocking the normal microtubule dynamics has also been shown to induce cell apoptosis. Docetaxel travels in the body bound to plasma proteins including lipoproteins, α1 acid glycoprotein and albumin (46,47).

Cell Lines

PC3: Is one of the oldest and most studied prostate cancer cell lines. It was acquired from an adenocarcinoma at stage IV that metastasized to the bone in a 62 year old Caucasian man. PC3 is androgen independent and is considered to be a good model for HRPC. This cell line was first reported in 1979 and since has been extensively used. Today 11 sub cell lines have been derived from PC3 (48). Experiments involving the injection of the 4 x 10^5 cells into athymic nude mice show tumor growth on the site of injection which then metastasizes to the lymph nodes, prostate, lungs, bones and liver. The tumor size varies from 1 to 3 cm in diameter within 60 days (49).

LNCaP: Along with PC3, LNCaP is one of the oldest cell lines available for the study of prostate cancer. LNCaP has been widely studied, yielding 1,918 references in prostate cancer research. There have been more sub cell lines derived from LNCaP than any other prostate cancer cell line. This cell line was isolated from a lymph node metastatic lesion from a 50 year old Caucasian man. This cell line is significantly less aggressive than PC3, forming tumors only in 50% of nude mice when injected subcutaneously. This cell line also requires an addition of matrix collagen formulations to promote tumor growth (48).

LNCaP CL1: This cell line (herein referred as CL1), was derived from LNCaP by growing the cells depleted from androgen in the medium. 10% charcoal is used to strip the serum from androgen and the cell line is maintained androgen deprived. The transformed cell line is now much more aggressive than its predecessor. Unlike LNCaP, CL1 does not require the addition of matrix collagen formulations to effectively form tumors. CL1 cells injected subcutaneously induce tumors within 2 weeks in 100% of nude mice. This cell line also metastasizes to the lungs, liver, spleen, lymph nodes, kidney, brain and bone (48,50).

With these 3 cell lines we can evaluate changes in metastatic potential starting from LNCaP, the non-metastatic, followed by PC3 the intermediate, and ending with CL1 the most aggressive.

Hypotheses

We hypothesize that: (a) highly metastatic prostate cancer cells express more plasma membrane V-ATPase compared to poorly metastatic prostate cancer cells; (b) highly metastatic cells extrude acid from the cell at faster rates than poorly metastatic cells due to the increased levels of pmV-ATPase; (c) V-ATPase activity in isolated plasma membranes from highly metastatic prostate cancer cells will be greater than in poorly metastatic cells; and (d) inhibition of plasma membrane V-ATPase enhances the efficiency of Docetaxel to kill prostate cancer.

CHAPTER II

METHODOLOGY

Cell Culturing

The prostate cancer cell lines LNCaP, PC3 and CL1 obtained from the American Type Culture Collection (ATCC). LNCaP cells were grown in RPMI media supplemented with 10% Fetal Bovine Serum (FBS) and 1% penicillin: streptomycin solution. CL1 cells were grown in RPMI media supplemented with 5% charcoal-treated serum, 1% (v/v) L-glutamine, 1% pyruvate, 1% nonessential aminoacids and 1% penicillin: streptomycin solution. For cell passage, all cells were treated with trypsin at 37°C for 2 minutes. These cells were grown in T-75 culture flasks and passed weekly at inoculation density of 2-3 x 10^4 cells per 75 cm^2. These cells were maintained at 5% CO_2 atmosphere at 37°C.

Intracellular pH measurements using SNARF-1

Intracellular pH was determined by the fluorescence of SNARF-1 (5-[and-6] carboxy-SNARF-1) as described previously (51). SNARF-1 is membrane permeable in the acetoxymethylester (AM) form. Once in the cell the dye is cleaved by cell esterases to produce the free acid form of the dye, which is membrane impermeable. Two cover slips containing cells at 80-90% confluency were placed into a 30 mm petri dish with 2 ml of cell superfusion buffer (CSB: 0.44 mM KH_2PO_4, 110 mM NaCl, 0.35 mM Na_2HPO_4, 1.3 mM $CaCl_2$, 1 mM $MgSO_4$, 5.4 mM KCl, 25 mM HEPES, 5 mM Glucose, 2 mM L-Glutamine, pH 7.4) and 7.5 µM SNARF-1-AM and incubated at 37°C in 5% $C0_2$ for 30 minutes on a rocker platform (Cole-Parmer, Vernon Hills, IL). The cells were then rinsed with CSB, and further incubated in CSB at the pH being studied for 5 minutes at 37°C in 5% CO_2 to ensure complete ester hydrolysis and leakage of uncleaved dye.

The two cover slips were placed back-to-back in a holder perfusion device and perfused at a rate of 3ml/min and the fluorescence of SNARF-1 was monitored with a SLM-8100/DMX spectrofluorometer (Spectronics Instruments, Rochester, NY) equipped for sample perfusion.

The sample temperature was maintained at 37°C by keeping both the water jacket and perfusion media at 37°C using an iso-temperature immersion circulator water bath (Lauda model RM20, Brinkmann Instruments, Westbury, NY).

All measurements were performed using 4 nm-bandpass slits and an external rhodamine standard as a reference Fluorescence was monitored in continuous acquisition mode by using an excitation wavelength of 534 nm and monitoring emissions at 584, 600, 644 nm (51). The fluorescence emission at 584 nm decreases and that at 644 nm increases with increasing pH; as such the ratio of 644/584 was used to monitor pH changes. The 600 nm wavelength, which is insensitive to pH, was used to evaluate the efficiency of dye loading, quenching or other artifacts. Fluorescence data were converted to ASCII format for analyses.

In situ calibration: In situ calibration curves were generated as described previously (51). Briefly, the cells attached to cover slips were perfused with High K+ buffer (NaCl 10 mM, KCl 146 mM, HEPES 10 mM, MES 10 mM, Bicine 10 mM, 2 μM valinomycin and 6.8 μM nigericin, Glucose 5 mM, Glutamine 2 mM, pH 5.5 to 8.0 adjusted with NaOH). The buffer contains high K^+ to approximate intracellular K^+ concentration. Nigericin is an ionophore which exchanges H+ and K+ across the membrane rendering the intracellular pH (pH_i) equal to the extracellular pH (pHex). Valinomysin is an ionophore which moves K^+ across the plasma membrane and helps to equilibrate $pH_i = pH_{ex}$.

The pH of the buffers was determined using a Beckman pH meter with a glass electrode (Corning Inc., Horseheads, NY) calibrated at 37°C with commercially available standard solutions (VWR Scientific, San Francisco, CA). The ratio (R=644/584) of SNARF-1 was converted to pHi using a modified Henderson-Hasselbalch equation.

$$pH = pKa + \log\left[\frac{Robs - Rmin}{Rmax - Robs}\right] \quad (1)$$

Where Robs was the ratio observed at any given pH, R_{min} was the ratio observed when the dye was fully protonated. R_{max} was the ratio observed when the dye was fully deprotonated.

The equation was solved using nonlinear least squares analysis with Sigma Plot to obtain the values of pKa, R_{min}, and R_{max} for SNARF-1 in these cells. The in situ calibration parameters were used to generate the pH_i (intracellular pH), values for each individual experiment by using equation (1) with Sigma Plot (version 10).

Proton Fluxes

The initial rate of recovery from an acetate induced acid load was measured as dpH/dt, as described previously (52). To determine dpH/dt we looked at recovery of pH in the first 3 minutes following acid loading by perfusing Na-free K-acetate CSB (herein referred as K^+-acetate buffer, 0.44 mM KH_2PO4, 1.3 mM $CaCl_2$, 1 mM $MgSO_4$, 5.4 mM KCl, 25mM HEPES, N-methyl Glucamine 60 mM, K-acetate 50 mM, 5 mM Glucose, 2 mM L-Glucamine, pH 7.4) at a rate of 3 ml per minute. The individual data points were subtracted from the steady state pH_i at five minutes and plotted against time. These points where then used to construct a linear regression curve relating time and delta pH (dpH/dt) (53). We calculated the proton fluxes (J_{H+}) by multiplying the apparent buffering capacity (bi) x dpH/dt as described previously (51).

$$J(H+) = bi\ (apparent)\ x \frac{dpH}{dt} \qquad (2)$$

Immunocytochemistry

12mm round coverslips are placed on a 60 mm petri dish. Cells are plated and allowed to grow until 60% confluency. The cells are fixed with 4% paraformaldehyde, quenched with NH_4Cl and permeabilized with Triton 0.1% in PBS. The E subunit antibody (rabbit anti human) was diluted in PBS-BSA (1%) at 1:500. The primary antibody was incubated 1 hour at room temperature. The secondary antibody (goat anti rabbit red-568) was prepared at 1:500 along with the actin antibody at 1:200 (Alexa Fluor 488 Phalloidin). The actin antibody was used to

visualize the edges of the cell. Actin is a protein which forms microfilaments of the cytoskeleton. It is bound to the plasma membrane through linker proteins and allows us to see the edges of the cell clearly. Slides were imaged on two different confocal microscopes. Regular dual staining images were taken with the Zeiss LSM 510 Meta confocal microscope. Images analyzed with intensity correlation coefficient-based (ICCB) analysis were performed using the Nikon A1RMP multiphoton confocal microscope (54).

Plasma Membrane Purification

Cells were plated on 100 mm petri dishes and grown to confluency. 10 confluent plates were used to prepare a single sample of plasma membrane per cell line (about 50 million cells). Every step of the membrane purification process was done at 4°C. The cells were scrapped from the petri dishes using a rubber policeman and resuspension buffer (Tris 10 mM, EDTA 1 mM, NaCl 150 mM, Protease inhibitor cocktail (complete® 11 697 498 001; one tablet per 50 ml), pH 7.4). All the cells were combined into a single 15 ml conical tube and resuspended using homogenizing buffer (Tris 50 mM, Sucrose 250 mM, EDTA 2 mM, Protease inhibitor cocktail (complete® 11 697 498 001; one tablet per 50 ml), pH 7.3). The cells were homogenized using a Teflon/glass dounce homogenizer with 20 strokes. This homogenate (F2 fraction) was centrifuged at 300 x g (5 min at 4°C) to separate the nuclear fraction (F1 fraction). The supernatant (F3 fraction) was then centrifuged at 100,000 x g (45 min at 4°C) and resuspended in homogenizing buffer. A 20-40% discontinuous sucrose gradient in 10 mM Tris pH 7.4, 1 mM EDTA was prepared for the membrane separation. The resuspended pellet was carefully added to the top of the gradient and centrifuged at 100,000 x g (1 hour at 4°C). The interface containing our plasma membrane was then collected, centrifuged at 100,000 x g (30 min at 4°C) and resuspended in homogenizing buffer to obtain our plasma membrane sample. The samples were stored at -80°C.

Lowry Protein Assay

The reagents for Lowry protein assay are kept separate and combined at the time of the experiment. These are Lowry A (2% Na_2CO_3 in 0.1 M NaOH) Lowry B (1% $CuSO_4$ in ddiH_2O) and Lowry C (2% sodium potassium tartrate). The working reagent is prepared with

49 ml of Lowry A, 0.5 ml Lowry B and 0.5 ml of Lowry C. Our standard curve is prepared with BSA at a concentration of 1 mg/ml and diluted in ddiH_2O to provide for 6 points in the standard curve ranging from 0 mg/ml to 50 mg/ml. Each of our plasma membrane samples were tested by diluting the amount of sample to 100 μl in water per tube. Each sample was measured in duplicates and in 2 different concentrations. To each sample 900 μl of the working Lowry reagent was added after which 50 μl of Folin's reagent were added. Absorption of each sample was read using a spectrophotometer at 550 nm (55).

Western Blot

Polyacrylamide 4-20% continuous gels were obtained pre cast from Bio-Rad. Electrophoresis (25 mM Tris, 192 mM Glycine, 0.1% SDS, pH 8.3) and Transfer buffers (20 mM Tris, 192 mM glycine, 20% methanol, pH 8.3) were purchased at 10x concentration from Bio-Rad and diluted at the time of the experiment. PBS-Tween 0.1% was also prepared at the time of the experiment. Plasma membrane samples were loaded in the SDS-PAGE gels in duplicates with 25 and 50 μg of protein per well. Each plasma membrane sample was prepared for testing by diluting 1:1 with Laemmli buffer containing 1% β-mercaptoethanol. The samples were heated to 100°C for 5 minutes to denature the proteins. The migration was done at 100 V until the bromophenol blue of the laemmli buffer reached the bottom of the gels. The transfer was done at 100 V for 1 hour. The nitrocellulose membranes were blocked in PBS-Tween with 3% milk (instant non-fat dry milk) overnight at 4°C. The nitrocellulose membranes were washed 3 times in between each antibody incubation. The antibodies were diluted in PBS-Tween with milk 3% at a concentration of 1:5000 for the α subunit of Na^+/K^+ ATPase (mouse anti human). The secondary antibody is goat anti mouse (680 nm) and was diluted in PBS-Tween with milk 3% at 1:6000 dilution. The incubation for the primary antibody was 12 hours at 4°C and 1 hour at room temperature for the secondary antibody. The nitrocellulose membranes were visualized using a LI-COR Odyssey Infrared Imaging System.

V-ATPase Activity Assay

For each plasma membrane sample, 5-30 μg of protein were tested. Each sample was added to a solution containing 3 mM ATP, 3 mM $MgSO_4$, 25 mM Tris-SO_4 (pH8), and 5 mM NaN_3.

This buffer does not contain either Calcium or Potassium in order to reduce the activities of several P-type ATPases. To test for V-ATPase specific activity, Bafilomycin 1 μM was added to a separate sample done at the same time. The samples were incubated at 37°C for 20 minutes. To stop the reaction 24% SDS was added. Inorganic phosphate was tested using a modified Chifflet's inorganic phosphate assay. The standard curve was prepared using different concentrations of K_2HPO_4 ranging from 0 μM to 100 μM. Reagent B (12% ascorbic acid in 1 N HCl, 200 μM EDTA), Reagent C (2% ammonium molybdate in 1 N HCl) were combined 1:1 at the time of experiment and added to each of the samples. Reagent E (2% Sodium Citrate, 2% sodium metarsenite, 2% acetic acid, dissolved in ddiH_2O) was then added and allowed to incubate for 20 minutes. Absorbance was read using a spectrophotometer at 850 nm (56,57).

QRT-PCR

To isolate RNA from the prostate cancer cell lines, QIAGEN RNeasy Mini Kit was used. Manufacturer protocol was followed. Total amount of RNA was measured using the NanoDrop spectrophotometer (absorbance at 230 nm). The verso cDNA kit (Thermo Scientific) was used to make cDNA from the RNA sample previously isolated. The reaction mix contained 1 μg of RNA, 5 X cDNA synthesis buffers, dNTP Mix, Anchored Oligo-dT to provide random primers, RT Enhancer mix, verso Enzyme mix, and water to a total volume of 20 μl per reaction. Using Bio-Rad MyIQ thermal cycler, the synthesis occurred for 1 hour at 42°C. The amount of cDNA synthesized was measured using the NanoDrop spectrophotometer (absorbance at 260 nm). SYBR® Green Master Mix (Applied Biosystems) was used for quantitative PCR (qPCR) on Bio-Rad's MyIQ thermal cycler. Primers for *a1, a2, a3* and *a4* isoforms were purchased from Thermo Scientific. To make accurate standard curves for the qPCR, plasmids with the genes of interest were purchased from Open Biosystems. Plasmid DNA was carried on E. Coli and was therefore isolated using the QIAGEN Mini Prep. Standard curves were prepared using 10-fold dilutions modified to cover the concentrations of the samples. The qPCR reaction mix contained the 2 X SYBR Green master mix, the primer set, 100 ng of cDNA template and water for a total volume of 25 μl. The

thermal cycler was run for 40 cycles of 1 minute at 62°C and 1 minute at 92°C. It was then followed by a melt curve to visualize any possible secondary amplicons (amplification product) on our sample. As a control, the levels of mRNA for the ribosomal protein S15 in all the cell lines were measured. The primers for S15 were provided by Dr. Stephanie Filleur. No plasmid was used to create a standard curve since we are not interested in measuring the exact levels of S15 mRNA. The samples were instead used as standard curves to compare between each other the levels of S15. The ribosomal protein S15 is a house keeping protein and is part of the 16S ribosomal RNA. It is involved in the rRNA-protein interactions along with the S8 ribosomal protein (58).

Cytotoxicity Assay

Each cell line was plated on 24-well plates and allowed to grow to 50% confluency. The cells were treated with Bafilomycin, Docetaxel or a combination of both. The drugs were diluted in warm media and added to the cells at the start of the experiment. The concentrations of each drug ranged from 500 nM to 1 nM plus the control (no drug). Bafilomycin and Docetaxel were tested in duplicates. Bafilomycin treatment of the cells showed that 10 nM only killed 80-90% of the cells so this concentration was used for the combined drug treatment. Treatment with the drug lasted for 48 hours after which the cells were fixed with 2% glutaraldehyde, washed with PBS, and stained with 0.1% crystal violet. The crystal violet of the cells was diluted using 10% acetic acid and the absorbance was read using FLUOstar OPTIMA.

Statistical Analysis

The software SigmaStat (version 3.5) was used to do the statistical analysis. For the comparison of two groups that showed a parametric distribution, the Student's t test was used. Mann-Whitney was used if the distribution was non parametric. One-way Analysis of Variance (ANOVA) was used for comparison of multiple groups. Holm-Sidak test was used when the distribution was normal and Dunn's test when the distribution was non-parametric.

CHAPTER III

RESULTS

In Situ Calibration of SNARF-1

In order to measure proton fluxes across in each of our cell lines, we must first calibrate the ratiometric fluoroprobe SNARF-1 using in situ titration. As shown in figure 2, the titration of buffers which change the intracellular pH (pH_i) from 5.5 to 8 (see methods) was fitted to a modified Henderson-Hasselback equation (equation 1) to obtain the pK_a, R_{max} and R_{min}.

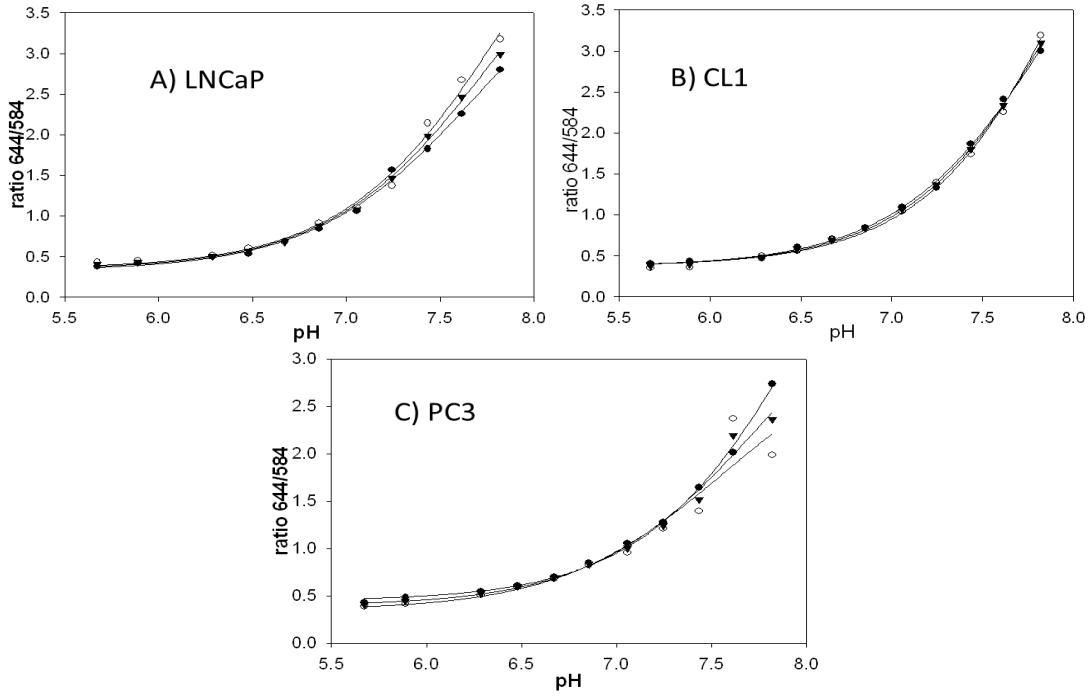

Figure 2: Titration curves for all prostate cancer cell lines. All cell lines were grown to sub-confluency and loaded with SNARF-1 and washed with CSB prior to analysis. Cells were perfused with high K^+ buffer with ranging pH of 5.5 to 8. The fluorescence ratio of SNARF was recorded for cell populations. A) LNCaP in situ titration curve gave an R_{min} of 0.3407, an R_{max} of 5.5540 and a pK_a of 7.7931. B) CL1 in situ titration curve gave an R_{min} of 0.3697, an R_{max} of 7.4919 and a pK_a of 8.0295. C) PC3 in situ titration gave an R_{min} of 0.3932, an R_{max} of 4.21338 and a pK_a of 7.7576. n=3

There are several factors that can alter these values, some of these include the protein concentration in the cell and the viscosity of the intracellular environment (51). Performing in situ titration on all our cell lines allows us to correct for these differences. The R_{max} values of the cell lines were not obtained experimentally since the cells cannot withstand such alkaline pH. The R_{max} values were predicted after the fitting of the modified Henderson-Hasslebalch equation.

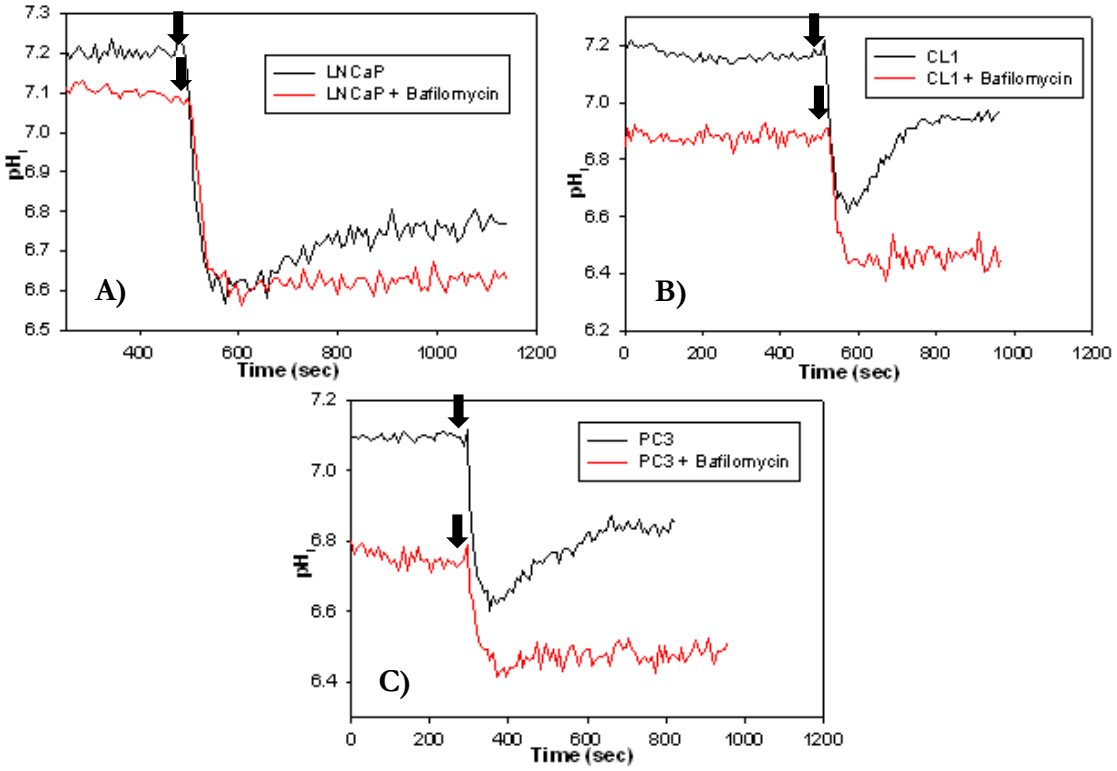

Figure 3: Changes of pH_i over time on LNCaP, PC3 and CL1. Cells were loaded with SNARF as described in the methods. K^+-Acetate buffer was added at the time shown by the arrows. A) LNCaP changes in pH_i show little recovery after an acid load. B) CL1 changes in pH_i show a much greater pH_i recovery than LNCaP while keeping the same steady state pH_i. C) PC3 cells have a slightly more acidic pH_i than the other cell lines while having a pH_i recovery that seems to be intermediate. The red tracing represents the changes in pHi after pre-incubation with 1μM bafilomycin for all cell lines. With bafilomycin, all steady state pH_i is more acidic while inhibiting the recovery after the addition of K^+-Acetate buffer. These figures are representative of 7 separate experiments per cell line.

Proton Fluxes

In order to study the ability of the V-ATPase to regulate pH_i, we measured the changes in pH_i after an acid load. The steady state pH_i was obtained by perfusing the cells with CSB and the acid load was done by perfusing with K^+-Acetate buffer.

In figure 3 we show representative data for the effect of acid loading in cells treated with bafilomycin, to inhibit V-ATPase, as well as in non-treated controls. These data shows that 10 μM Bafilomycin is sufficient to inhibit the ability of the cells to recover from acid loads. Notice the pre-incubation of cells with bafilomycin results in cells exhibiting lower pH_i than non-treated controls. The changes of pH_i before and after an acid load provided us with enough information to calculate proton fluxes. The apparent buffering capacity was multiplied to the change in pH_i over time (dpH_i/dt) after an acid load to obtain the proton fluxes (see methods).

Figure 4 shows that CL1 has 3 times faster J_{H+} than LNCaP whereas PC3 cells have intermediate J_{H+}. The steady state pH_i of all three cell lines is not significantly different and serve as a control for baseline pH_i regulation.

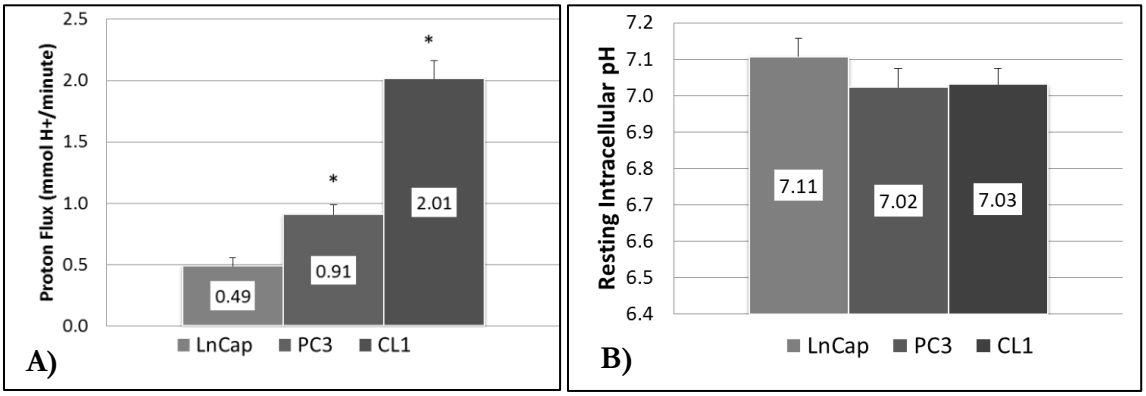

Figure 4 Proton fluxes and resting pH_i. A) All proton fluxes (J_{H+}) are expressed in milli moles of proton per minute (mmol H^+/min). LNCaP and PC3 have an n=12, while CL1 has an n=16. CL1 shows 3 times faster proton fluxes than LNCaP, and twice faster than PC3. Error bars show the standard error of the mean. B) The steady state pH_i of all the cell lines is not significantly different from one another. * $P<0.001$ when comparing all cell lines to each other.

Plasma Membrane V-ATPase Activity

To study the V-ATPase activity at the plasma membrane we obtained enriched plasma membrane fractions. These samples were obtained by subcellular fractionation using sucrose gradients and cell homogenates. To demonstrate the enrichment of plasma membrane purification, we evaluated by Western blot labeling for the Na^+/K^+ ATPase (a plasma membrane marker) using samples from each step in the plasma membrane purification (59). The samples were the total cell homogenate (F2 fraction) which was then separated into two fractions, the supernatant (F3 fraction) and the nuclear fraction (F1 fraction). We expect that the nuclear fraction should contain little to no amount of Na^+/K^+ ATPase whereas the plasma membrane should be enriched with this enzyme. Figure 5 shows that we see progressively more Na^+/K^+ ATPase starting from the nuclear fraction, followed by the total cell homogenate and the cell homogenate. The isolated plasma membrane fractions contain the highest amount of Na^+/K^+ ATPase consistent with higher enrichment of plasma membranes.

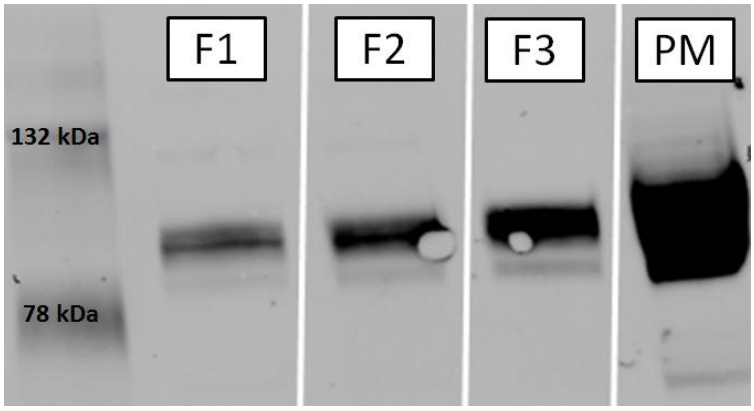

Figure 5: Detection of Na^+/K^+ ATPase in different steps of plasma membrane purification using western blot. Plasma membrane was isolated through sucrose gradient centrifugation. Samples were taken at each step of the purification process and were tested on a western blot labeling for the plasma membrane marker Na^+/K^+ ATPase. F1: nuclear fraction. F2: Total Cell Homogenate. F3: Supernatant containing the fraction of the total cell homogenate without the nucleus and mitochondria. PM: Plasma membrane sample. This shows that the plasma membrane is enriched with Na^+/K^+ ATPase allowing us to conclude that we have enriched plasma membrane. Gels were loaded with 50 μg of protein per lane.

To test for ATPase activity in the plasma membrane we used a modified version of Chifflet's inorganic phosphate assay (57). This assay allows us to measure the amount of inorganic phosphate produced by the ATPases in the presence of ATP over a period of time. The activity buffer contains all the reactants needed for enzymatic activity (see methods). Bafilomycin was used to inhibit V-ATPase activity. The difference between the total activity and the Bafilomycin sensitive activity was the V-ATPase specific activity.

The modified version of Chifflet's inorganic phosphate assay is highly sensitive, producing color with as little as 5 μM inorganic phosphate, and sustains a linear relationship with absorbance up to 360 μM as shown in figure 6. Samples remain stable up to six hours, reducing the possibility of absorbance changes when reading the samples.

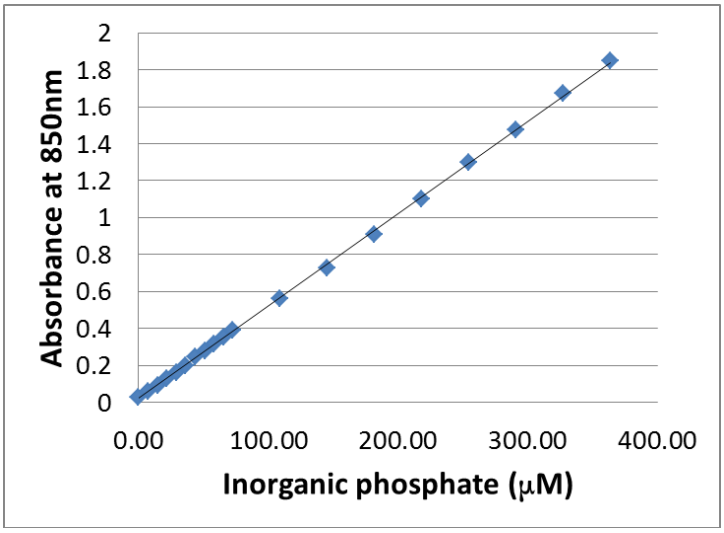

Figure 6: Chifflet's modified inorganic phosphate assay sensitivity. Samples with increasing concentration of K_2PO_4 were tested with the modified inorganic phosphate assay to test the sensitivity of the assay. Sensitivity starts from 5 μM of inorganic phosphate. Increasing concentration sustains linearity with absorbance at 850nm up to 360 μM making this assay very accurate. Precision is detected within 2 μM difference.

V-ATPase specific activity is shown in figure 7 for LNCaP, PC3 and CL1. Notice that CL1 shows significantly more V-ATPase activity than any other cell type at 170.64 μM Pi/mg protein/min. This is almost 7 times higher than what is observed in LNCaP (26 μM Pi/mg

protein/min). The activity for PC3 was expected to be in between LNCaP and CL1, but our results show that there is no statistical difference between PC3 and LNCaP. It has been shown that V-ATPase can help regulate vesicular recycling which may account for the increased proton fluxes seen previously (35,36). All the experiments were done in duplicates with plasma membrane isolated on 5 different cell passages.

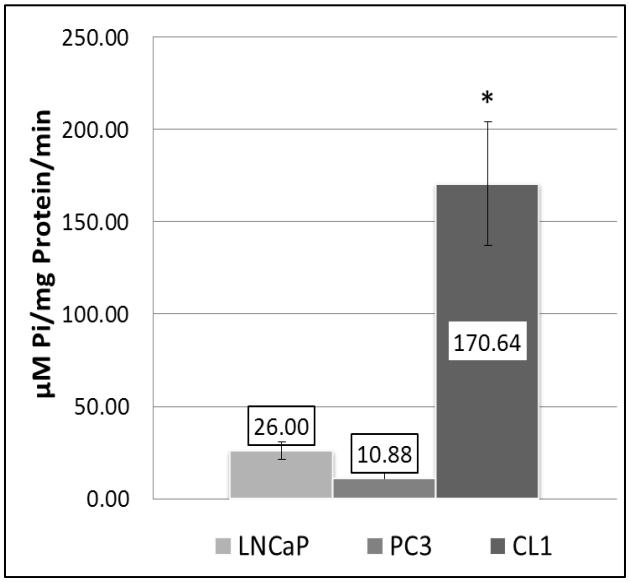

Figure 7: pmV-ATPase activity for CL1, PC3 and LNCaP. Plasma membrane enriched samples were tested for activity in solution containing MgSO4, ATP, NaN_3, Tris pH 7.4 at 37°C for 20 minutes. The activity for all cell lines was tested with and without Bafilomycin. Inorganic phosphate produced was measured as described in figure 6. The difference between activities with and without bafilomycin shows V-ATPase specific activity. CL1 shows almost 7 times more activity than LNCaP and PC3. Difference between LNCaP and PC3 is not statistically significant. All experiments were run twice per sample. Plasma membrane samples were obtained on 5 different days making the n=5 for each cell line. * $P<0.001$

QRT-PCR

Isoforms of the *a* subunit of the V-ATPase have been associated with targeting of the V-ATPase to different subcellular organelles. The isoforms *a1* and *a2* have been shown to target the V-ATPase to intracellular vesicles. Both isoforms *a3* and *a4* target the V-ATPase to the plasma membrane (28). To determine mRNA levels of these subunits we performed

Quantitative Reverse-Transcription Polymerase Chain Reaction (QRT-PCR). The mRNA levels for the ribosomal protein S15 were used as a control. Since no plasmid was used to determine the correct amounts of S15 mRNA, the test samples were used to determine the relative amounts compared to one another. RNA isolated from 3 different cell passages was tested.

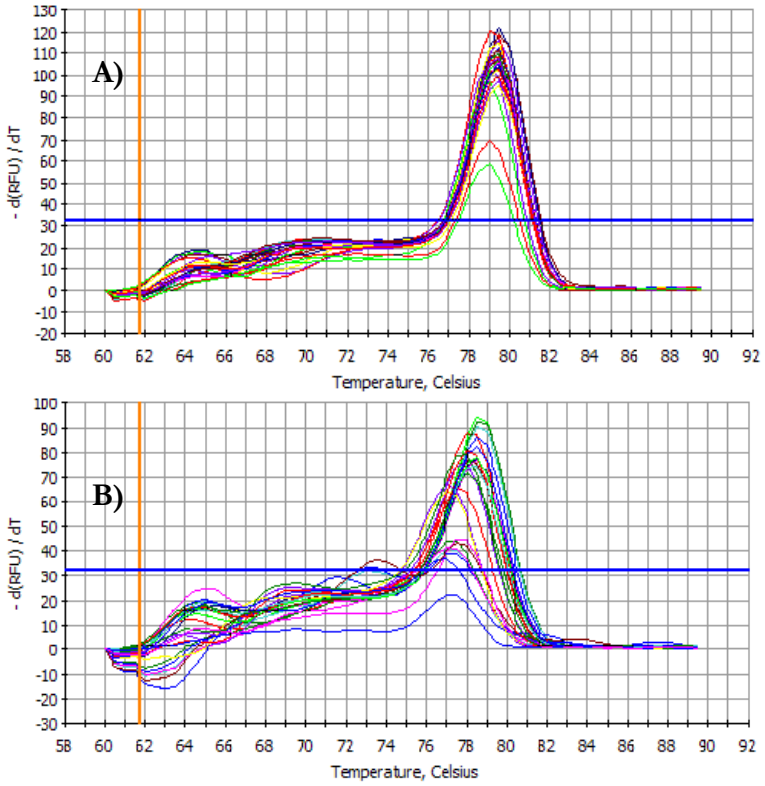

Figure 8: Melt curves for S15 and *a1* isoform. Melt curves allows to distinguish amplicons with different sequences and lengths. A single peak is shown when there is only a single product after amplification. A) S15 melt curve. B) *a1* isoform melt curve. All melt curves show a single peak.

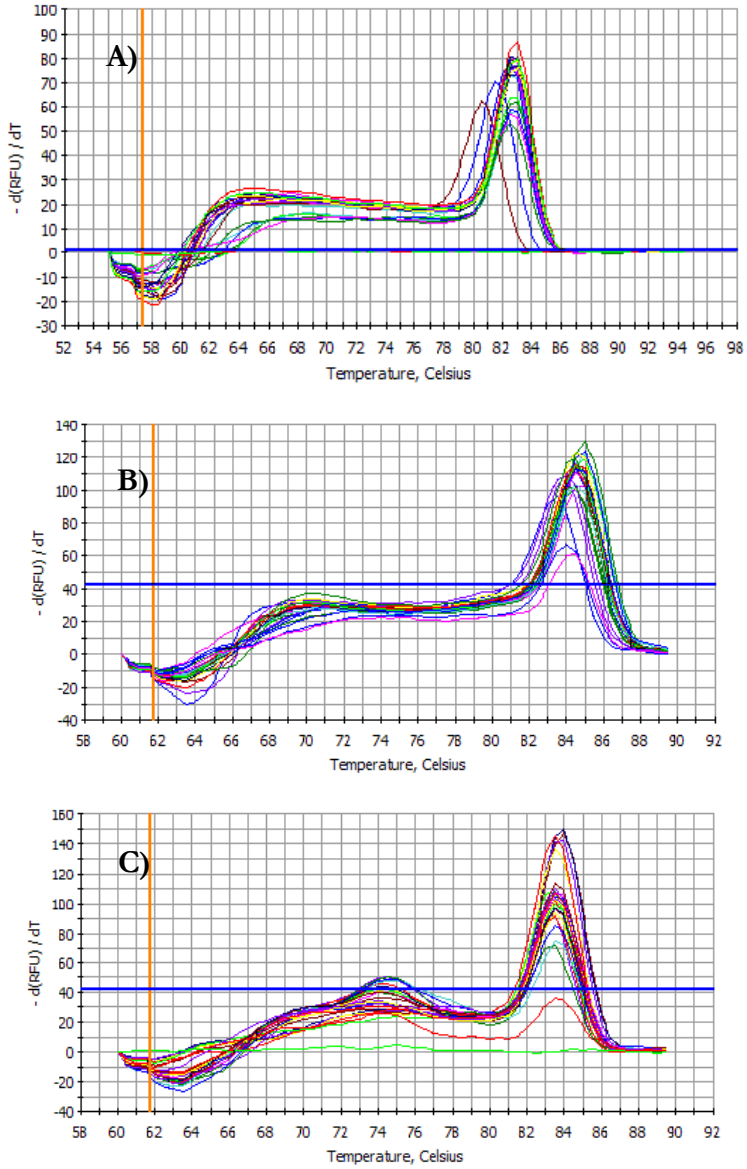

Figure 9: Melt curves for isoforms *a2*, *a3*, and *a4*. Melt curves allows to distinguish amplicons with different sequences and lengths. A single peak is shown when there is only a single product after amplification. A) *a2* isoform melt curve. B) *a3* isoform melt curve. C) *a4* isoform melt curve. All melt curves show a single peak.

To insure that the amplification is not producing a more than one amplification product, a melt curve was performed. A melt curve is performed by increasing the temperature of the

sample from a determined baseline in increments of 2-4°C. Double stranded DNA denatures at different temperatures depending on their adenine/thymine (A/T) versus guanine/cytosine (G/C) composition. Since guanine makes 3 hydrogen bonds with cytosine it is more stable than adenine and thymine which can only make two. This stability is compounded with more C/G pairs in sequence. The length of the double stranded DNA also changes the denaturing temperature. Longer DNA stands will require higher temperatures to completely denature (60). Figure 8 and 9 show a single peak in each of the melt curves for LNCaP, PC3 and CL1 in all *a* isoforms. This demonstrates that there is only one amplicons and that there are no contaminants. Samples that did not reach the threshold in the melt curve were discarded and repeated.

Figure 10 shows the amount of mRNA (in Nano grams) for each isoform per cell line. From these results we can see that in all the cell lines, there is more mRNA for the *a2* and *a3* isoforms than there is for *a1* and *a4*. The difference in mRNA amounts between *a2* and *a3* in CL1 and LNCaP is not statistically significant. However, the difference is significant in PC3. From this data we can see that LNCaP has the highest amount of mRNA for the *a1* isoform and the lowest amount of *a4* isoform. PC3 has the highest amount of both *a3* and *a4* isoforms and the lowest amount of *a1* isoform.

It is difficult to interpret the data provided by the mRNA levels between these cell lines. However, considering that the total expression of V-ATPase changes between cell lines, the ratio between the different isoforms can provide us with a better picture of how much of the V-ATPase produced is targeted to the plasma membrane.

Figure 11 shows the ratios of the amount of mRNA for *a4* isoform over *a1* and *a3* over *a1* in all the different cell lines. CL1 has almost 5 nanograms of *a4* mRNA per nanogram of *a1* giving it the highest ratio between the cell lines. PC3 follows with 1 nanogram of *a4* per 10 nanograms of *a1*. LNCaP has the lowest with 3.6 nanograms of *a4* per milligram of *a1*.

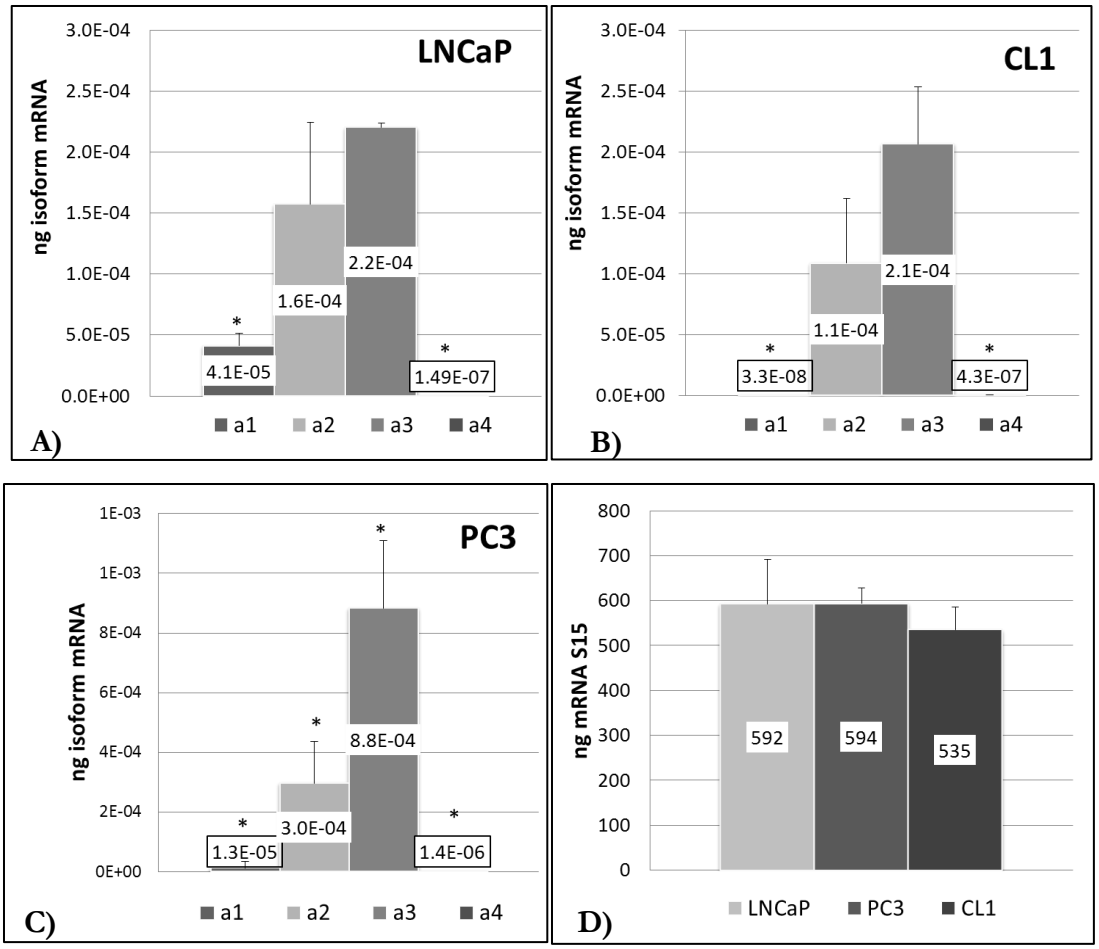

Figure 10: mRNA amounts for *a* isoforms and S15 in LNCaP, CL1 and PC3. The mRNA for each cell line was quantified using QRT-PCR. A) LNCaP mRNA amounts for all *a* isoforms. There is no statistical difference between *a2* and *a4* mRNA amounts. LNCaP has the highest amount of *a1* isoform compared to the other cell lines while having the lowest amount of *a4*. B) CL1 mRNA amounts for all *a* isoforms. There is no statistical difference between *a2* and *a3* mRNA amounts. C) PCR mRNA amounts for all *a* isoforms. PC3 has the highest amounts of both *a4* and *a3* mRNA. D) S15 mRNA levels. S15 is used as a control and there is no difference in amounts between LNCaP, PC3 and CL1. *P<0.001 n=3 for all cell lines

Regarding *a3*, CL1 has almost 2.5 milligrams of *a3* per nanogram of *a1*. PC3 has almost 70 nanograms of *a3* per nanogram of *a1*. LNCaP has only 5 nanograms of *a3* per nanogram of *a1*. The results are consistent with the predicted amounts of *a3* and *a4* isoforms which target the

V-ATPase to the plasma membrane. The amounts of mRNA for *a3* are much higher than those of *a4* which could reflect the significance of the *a3* isoform for metastatic potential.

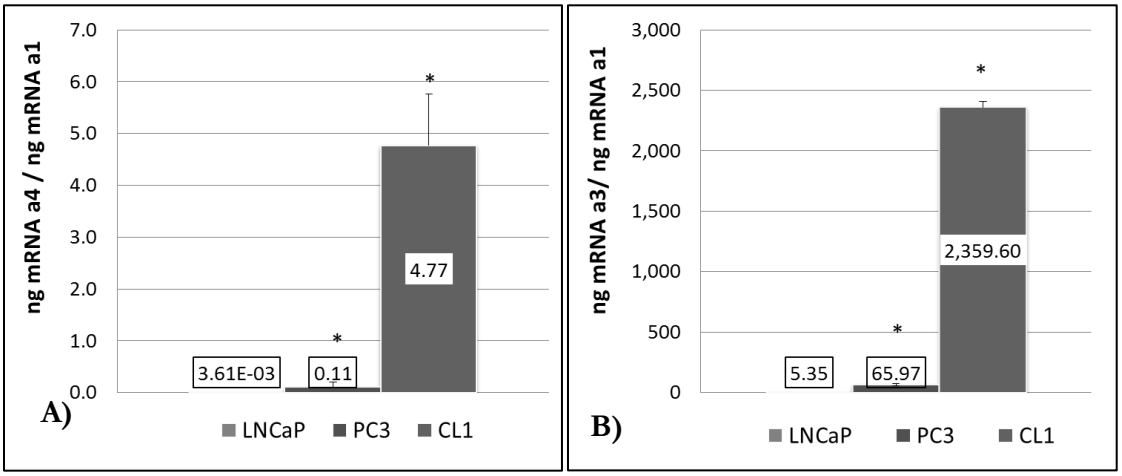

Figure 11: Ratio of *a4/a1* and *a3/a1* mRNA amounts (ng) for LNCaP, PC3 and CL1. A) ratio of nanograms of mRNA of *a4* over *a1* for all cell lines. CL1 has the highest ratio followed by PC3 and LNCaP. B) Ratio of nanograms of mRNA of *a3* over *a1* for all cell lines. The same pattern is observed here with CL1 being the highest and LNCaP being the lowest. We can see that there is much more *a3/a1* on all cell lines than *a4/a1*. This could show that *a3* is more significant for the change in metastatic potential than *a4*. n=3 *P<0.001

Immunocytochemistry

Immunocytochemistry was used to visualize the distribution of V-ATPase in the cell. Phalloidin was used to label actin and to be able to visualize the edges of the cell. At least 200 cells were visualized to study the distribution of the V-ATPase in each cell line. Figure 12 shows representative images from each of the cell lines.

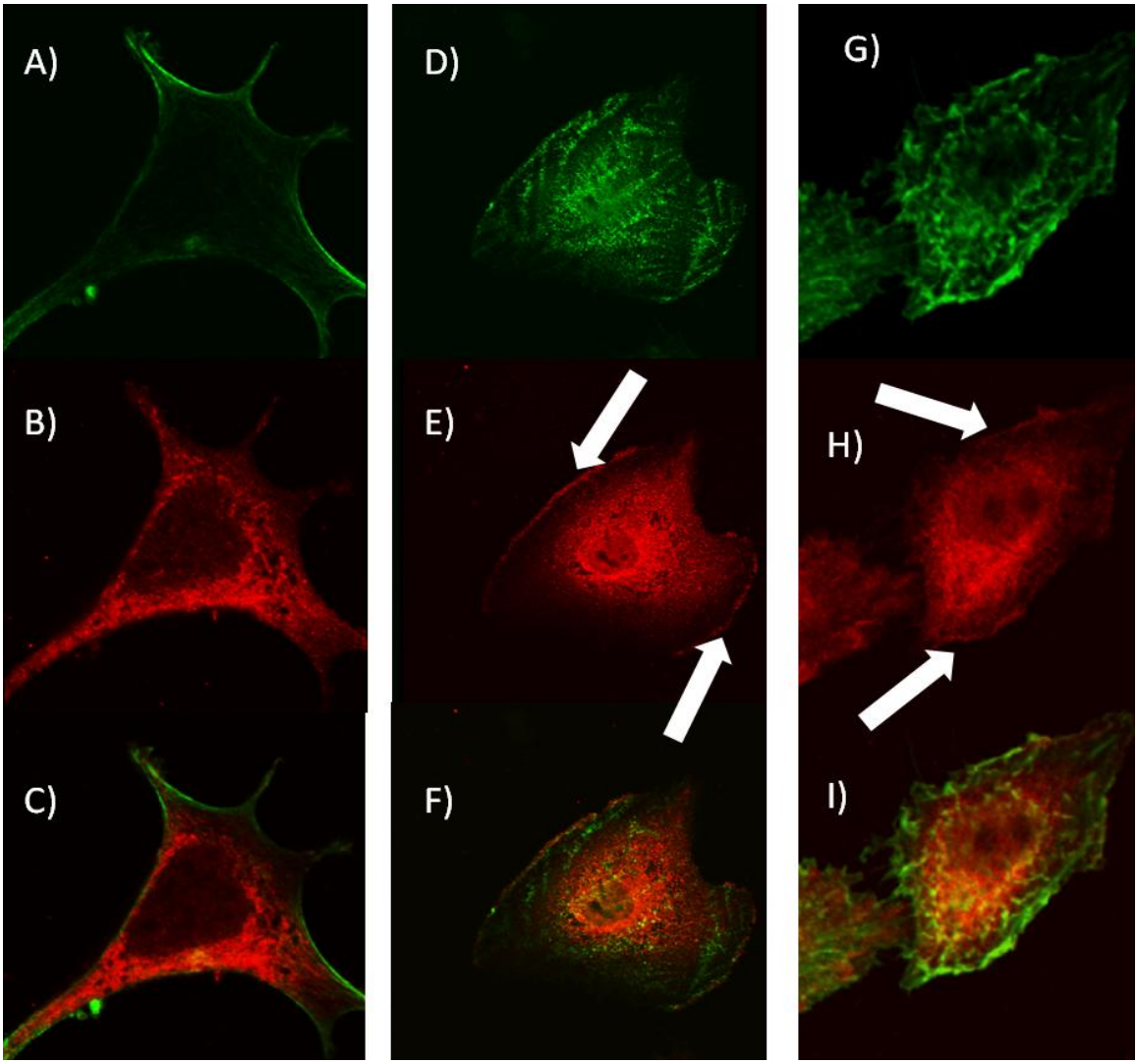

Figure 12: Actin and E-subunit staining in LNCaP, CL1 and PC3. All cell lines were grown to 60% confluency. They were then fixed with paraformaldehyde and permeabilized with 0.1% triton. The cells were washed with PBS in between each step. A-C) LNCaP, D-F) CL1, G) PC3. A) LNCaP labeled with actin to show the edges of the cell. B) Staining for the E subunit of the V-ATPase. C) Superimposition of the two stains shows no colocalization between the actin at the cell surface and the E-subunit of the V-ATPase. D) CL1 stained with actin to show the cell edges. E) CL1 stained for the E subunit of V-ATPase. V-ATPase can be seen accumulated at the edges of the cell. F) Superimposition of the two stains shows that there is colocalization of actin at the cell surface and the E subunit of V-ATPase. G) PC3 shows accumulation of the E-subunit at the edges of the cell.

As is expected, all the cell lines show punctuated distribution when labeled with the E subunit of the V-ATPases, since most of these proton pumps are found on acidic vesicles. PC3 and CL1 show distribution of the E-subunit at the edges of the cell that are clearly seen without the staining of actin. When the images staining for both E subunit and actin for CL1 and PC3 are super imposed, we can see that they are in proximity to each other. LNCaP on the other hand does not show distribution of the E subunit of the V-ATPase at the cell surface.

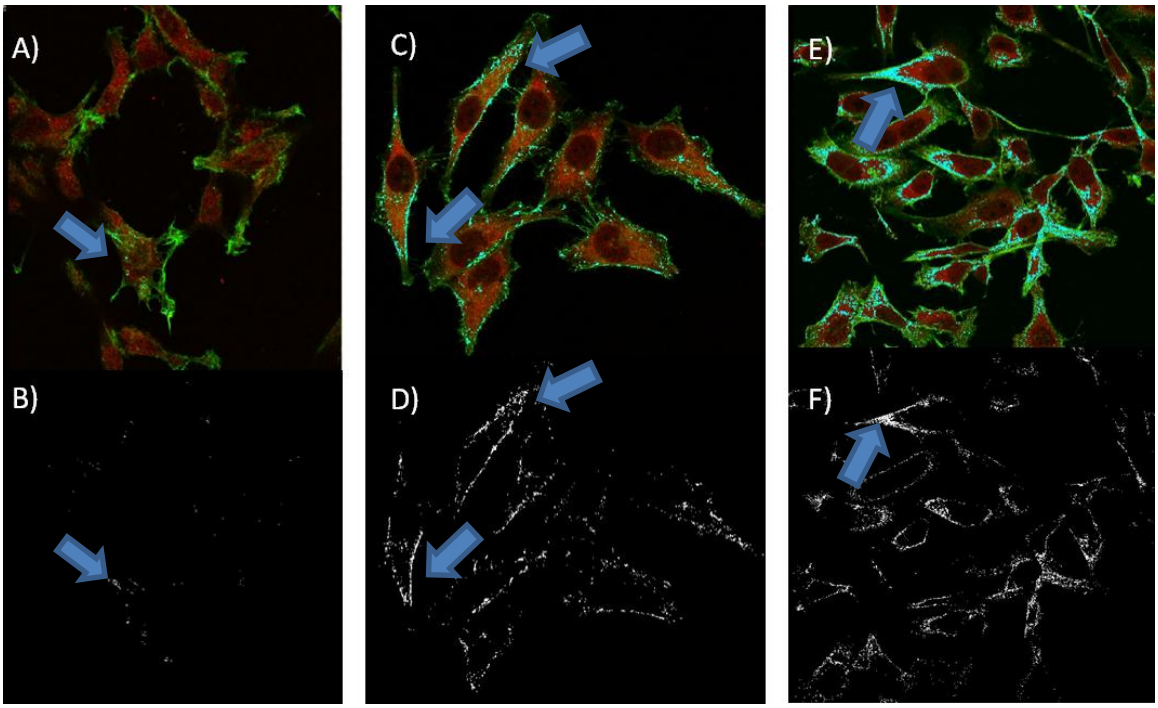

Figure 13: Actin and E-subunit colocalization in LNCaP, CL1 and PC3. Samples were prepared as shown in figure 11. Colocalization was calculated using intensity correlation coefficient based analysis on the Nikon A1RMP. A-B) LNCaP, C-D) CL1, E-F) PC3. A) LNCaP superimposition of actin and the E subunit of V-ATPase. B) Colocalization shows only minor areas of colocalization. C) CL1 superimposition of actin and the E subunit of V-ATPase. D) Colocalization in CL1 cells shows the presence of the E subunit of the V-ATPase at the edge of the cell. E) PC3 superimposition of actin and the E subunit of V-ATPase. F) Colocalization in PC3 cells shows the presence of the E subunit of the V-ATPase at the edge of the cell.

The superimposed image of both stains shows a clear delineation of the cell by actin while keeping all the punctuated bodies inside the cell. We can safely assume that in LNCaP there is no V-ATPase at the cell surface.

However, considering the limitations of confocal microscopy (61), conclusions regarding the colocalization of actin and the V-ATPase cannot be definitive. To obtain a better understanding of colocalization we performed intensity correlation coefficient based analysis on the images studied. In figure 13 we can see that only the PC3 and CL1 cell lines show colocalization at the edges of the cell while LNCaP shows little to no colocalization of the V-ATPase with actin.

Cytotoxicity

Based on the results from this study, there is an overexpression of V-ATPase at the plasma membrane which occurs as the prostate cancer cell becomes more aggressive. This led us to the hypothesis that inhibiting the V-ATPase can have a positive effect on the treatment of prostate cancer with the commonly used chemotherapeutic drug Docetaxel. However, the V-ATPase has a crucial role in the cell homeostasis. It is involved in pH regulation in acidic vesicles and in vesicle recycling. Since the V-ATPase is present in all cells in the body, blocking the activity of the V-ATPase alone in the treatment of prostate cancer is not a viable option. However, sub lethal dosages of the V-ATPase inhibitor bafilomycin can cause the cell to reduce the level of drug extrusion through vesicle recycling.

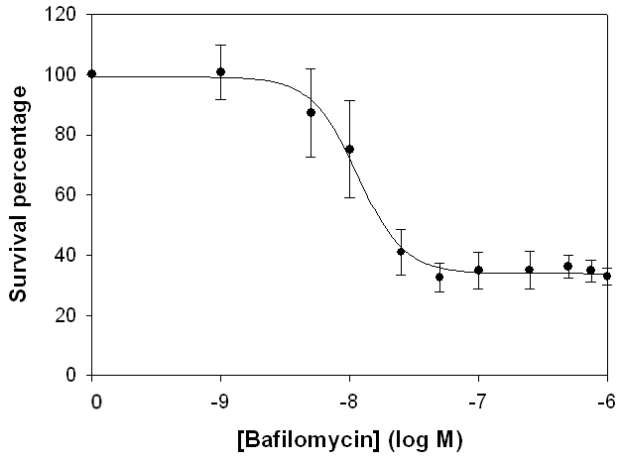

Figure 14: Dose-Response curve of LNCaP with Bafilomycin. This curve shows the survival rate of LNCaP cells under increasing concentrations of Bafilomycin. At 10 nM concentration of Bafilomycin, there is a survival percentage of 85% and was considered acceptable to use with Docetaxel. n=4

A cytotoxicity assay was performed on all cell lines to identify the sub lethal concentration of bafilomycin. Figure 14 shows the effect of bafilomycin at different concentrations in LNCaP. The concentration of bafilomycin started with 1 nM and increased until 1 μM. Bafilomycin at the concentration of 10 nM kills an average of 15% of the LNCaP cells and was considered a sub-toxic concentration to use with docetaxel.

In figure 15 we can see that 10 nM of bafilomycin causes the dose-response curves of Docetaxel for all the cell lines to shift to the left. This indicates that the IC_{50} (concentration of drug required to kill 50% of the cells) of docetaxel is reduced when adding 10 nM of bafilomycin. The largest decrease in IC_{50} is observed in the PC3 cell line, where 300 nM lower concentration of docetaxel is needed to kill 50% of the cells. LNCaP has the smallest drop in docetaxel IC_{50} with only a 0.9 nM difference. The IC_{50} of CL1 surprisingly only has a decrease of 1 nM in IC_{50} of docetaxel. These results can be seen in figure 16.

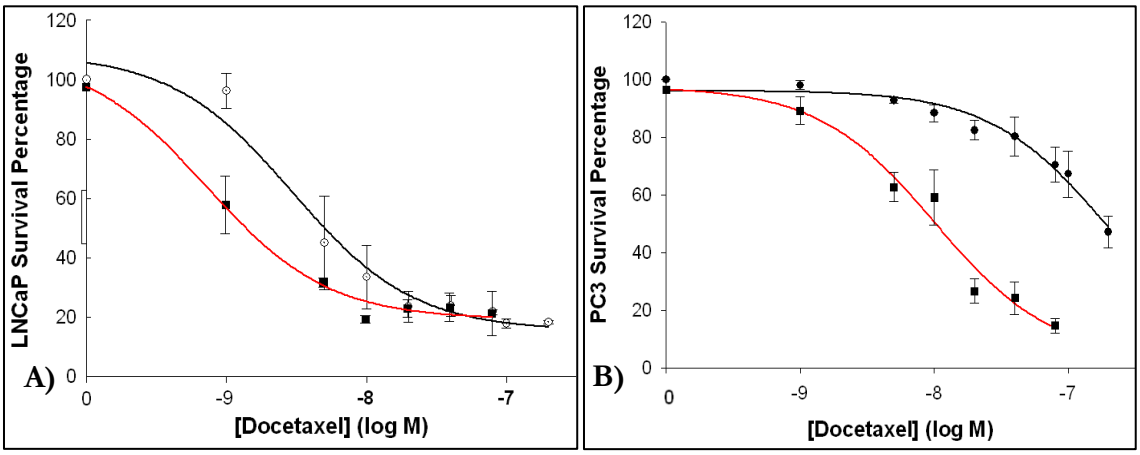

Figure 15: Dose response curves for LNCaP and PC3 under docetaxel with and without bafilomycin (10 nM). The cells were grown to 40% confluency before administering Docetaxel in increasing concentrations. After 48 hours of treatment, the cells were fixed with glutaraldehyde and stained with crystal violet. A) LNCaP cell survival to increasing concentrations of docetaxel alone (black) and with 10 nM bafilomycin (red). B) PC3 response to docetaxel alone (black) and with 10 nM bafilomycin (red). 10nM of bafilomycin is enough to cause a significant shift of the IC_{50}. n=4 for each cell line

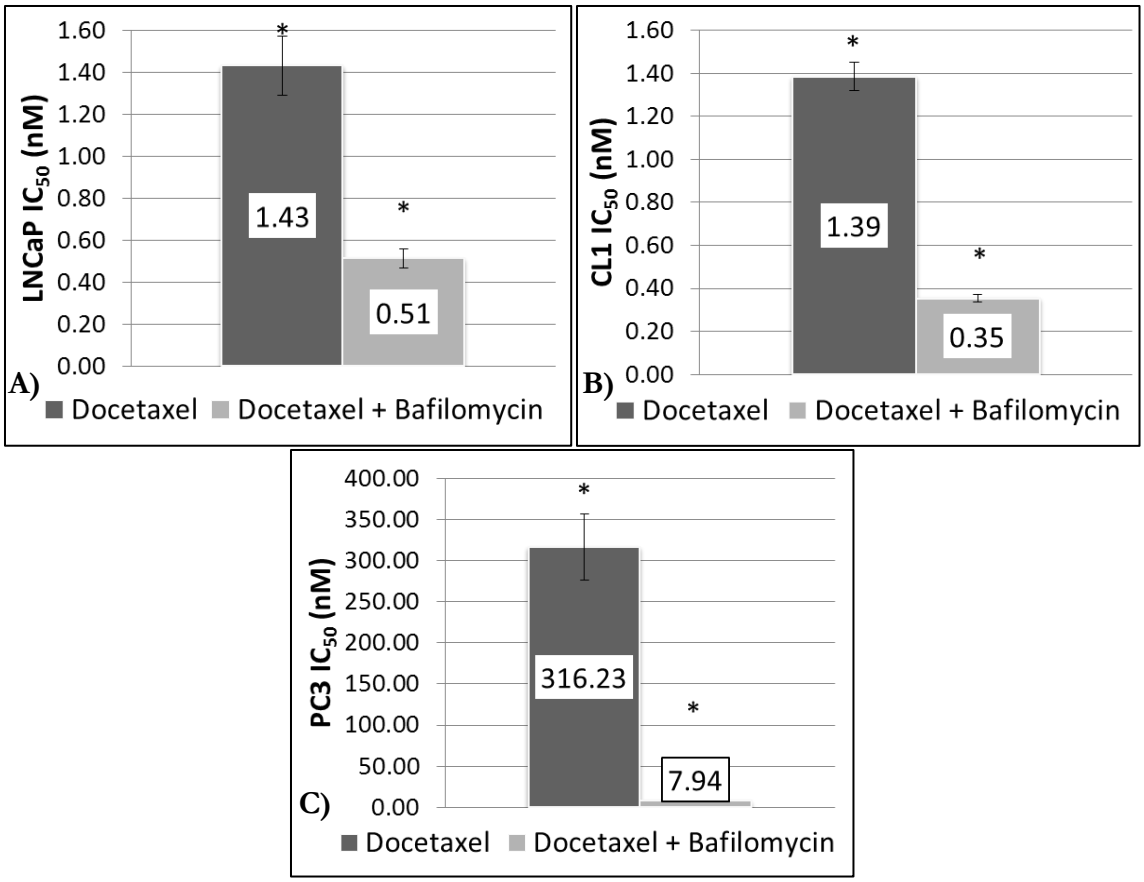

Figure 16: IC_{50} of docetaxel for LNCaP, PC3 and CL1 with and without 10 nM bafilomycin. The IC_{50} was calculated by fitting the cytotoxicity assay on a dose-response curve. A) The IC_{50} for docetaxel in the LNCaP cell line has the smallest change with only .9nM with the addition of 10 nM bafilomycin. B) CL1 IC_{50} for docetaxel only drops 1 nM with bafilomycin. C) PC3 has the highest change in IC_{50} with a 300 nM difference after the addition of 10 nM bafilomycin. * P=<0.001 n=4

CHAPTER IV

DISCUSSION

The V-ATPase is a proton pump essential for cell homeostasis. It is involved in pH regulation of the cell and acidification of acidic vesicles (i.e. endosomes and lysosomes). Even though its role in cancer has not been clearly established, it has been shown that its expression at the plasma membrane increases with metastatic potential in breast cancer cells (29).

Cancer cells have increased metabolism and rely mostly on glycolysis for their energetic needs. Due to poor vascularization and the increase in metabolic activity, the cell produces excess lactic acid. To prevent acidosis, the cancer cell expresses V-ATPases at the cell surface to extrude protons out of the cell. This increase in proton fluxes at the plasma membrane can also help in the ability of the cell to metastasize. The V-ATPase has the ability to regulate vesicular recycling. With the increased extrusion of cathepsins (protease found in the lysosomes), the plasma membrane V-ATPase can acidify the extracellular environment allowing it to digest the extracellular matrix (35,36). Using prostate cancer cell lines with different metastatic potential we can observe the changes in V-ATPase expression and activity as the cancer becomes highly metastatic. CL1 cells have the highest metastatic potential out of the three tested cell lines. They can form tumors in up to 7 distant sites, 3 more than the PC3 cell line. The LNCaP cell line forms local tumors and does not show signs of metastasis (48).

The pH fluoroprobe SNARF (5-[and-6] carboxy-SNARF-1) was used to determine the intracellular pH of the cells. This is a ratiometric fluoroprobe meaning that it has two different emissions depending if it is protonated or deprotonated. Since the cytoplasmic microenvironment changes in viscosity and protein composition between cell lines, the pK_a of the SNARF changes as well (62). This could be due to distinct diffusion mobility of the probe as has been seen previously in studies of fluorescence recovery after photo-bleaching (FRAP) (63). In situ titration allows us to determine the necessary values to correctly determine the pH in the cell while correcting for variations between the cell lines. Using a high K^+ buffer

containing nigericin and valinomycin we can change the intracellular pH to equal the extracellular pH (64).

The intracellular pH measured with SNARF shows that there is no significant difference in the resting pH between all the cell lines. However, the introduction of 10 μM bafilomycin to the cell produces acidosis. This is explained by the reduced ability of the cell to extrude acid through the plasma membrane V-ATPases. The introduction of acetate acidifies the cells and allows us to see the recovery of pH over time. The buffer containing acetate does not have sodium or bicarbonate to prevent the bicarbonate transporters and sodium proton exchangers to regulate intracellular pH (1). Under these settings we can see that the CL1 cell line has proton fluxes 3 times faster than LNCaP while PC3 is intermediate. This increase in proton fluxes correlates with the increasing metastatic potential of the cells. These proton fluxes are bafilomycin sensitive, providing evidence that the V-ATPase is the active player in the extrusion of acid from the cell.

Since the V-ATPase is found on the membrane of subcellular compartments as well as the plasma membrane, the purification of the plasma membrane can provide us with a picture of pmV-ATPase activity. The lipid to protein ratio of the plasma membrane is different than that of any other subcellular compartment. It is predicted that the plasma membrane is denser than the membrane from endosome and lysosomes. The density of the membrane found in the Golgi apparatus and the endoplasmic reticulum is less than that of the plasma membrane. Using sucrose gradient centrifugation we were able to separate the plasma membrane from the other membrane fractions (65). The Na^+/K^+ ATPase has been extensively studied and has been shown to be present at the plasma membrane (5,59). Using the Na^+/K^+ ATPase as a plasma membrane marker we were able to evaluate the enrichment of the plasma membrane purification. A sample of each step in the purification was tested in western blot staining against the Na^+/K^+ ATPase. The four samples tested correspond to a whole cell homogenate, a nuclear faction (containing the nucleus and mitochondria) and a homogenate. We observe that the nuclear fraction contains a trace amount of the Na^+/K^+ ATPase which can be attributed to membrane contaminants. The total cell homogenate is expected to follow after

the nuclear fraction since it includes the total amount of the Na^+/K^+ ATPase in the cell. The cell homogenate has been stripped from the nuclear fraction and shows the amount of Na^+/K^+ ATPase found in all membrane compartments. We can observe that the plasma membrane product contains a considerably high amount of the Na^+/K^+ ATPase and can be considered to be highly enriched.

With plasma membrane enriched samples we can test for activity specific to the pmV-ATPase. An ATPase activity can be measured by the amount of ATP that is hydrolyzed over a period of time. Chifflet's modified inorganic phosphate assay allows us to measure inorganic phosphate with high sensitivity. This assay can detect a minimum of 5 μM of inorganic phosphate and can detect changes of 2 μM between samples. ATPases require ATP, magnesium, a pH of 7.4 and a temperature of 37°C to work properly. We allowed 20 minutes of activity under these conditions to allow the LNCaP sample to produce enough inorganic phosphate for an accurate reading. The CL1 cell line produced 6.5 times more pmV-ATPase specific activity than what the LNCaP cell line produced. The pmV-ATPase activity for the PC3 cell line was expected to be somewhere in between the activities seen in CL1 and LNCaP. Instead we see that the activities between LNCaP and PC3 are not statistically different. The Proton flux experiment tells us that the PC3 cell line extrudes more acid than the LNCaP cell line. It also tells us that these fluxes can be suppressed with bafilomycin. However, as seen in previous studies, the V-ATPase can extrude acid by inducing an increase in vesicle recycling (21). This suggests that PC3 fluxes could be a result from increased vesicle recycling and not from increased expression of V-ATPase at the plasma membrane.

Previous studies show that isoforms for the *a* subunit in the V0 domain of the V-ATPase target the protein to different subcellular compartments. The *a1* and *a2* isoforms have been shown to target the V-ATPase to the intracellular vesicles. The *a3* isoform has been shown to target the V-ATPase to acidic vesicles that eventually fuse with the plasma membrane in osteoclasts. The *a4* isoform has been shown to target the V-ATPase to the plasma membrane in kidney cells. Studies in breast cancer show that the levels of mRNA for each isoform change when the cancer becomes metastatic (25,26,27,28).

QRT-PCR allows us to measure the amount of mRNA for each isoform on the different cell lines. Real time quantification measures amount of DNA regardless of what is being amplified. It is possible for the primers to be non-specific and amplify more than one gene. To test for more than a single amplicons we performed melt curves on the samples immediately after amplification. DNA can differ in denaturing temperature by length and by nucleotide composition. Longer DNA strands require higher temperatures to denature. DNA strands containing a high amount of G/C pairs have higher denaturing temperatures due to their 3 hydrogen bonds. None of the melt curves showed more than one peak which demonstrates that all the signal comes from denaturing at a single temperature. We can conclude that we only have a single amplicon per amplification. Using QRT-PCR we found that mRNA for *a2* and *a3* isoforms have the highest concentration. The *a1* and *a4* vary between the cell lines. Considering that most other subunits of the V-ATPase do not have multiple isoforms we can conclude that the ratio between the isoforms determines how much V-ATPase is targeted to the plasma membrane. CL1 cells have the highest amount of *a4* isoform mRNA and the lowest amount of *a1* mRNA while LNCaP has the opposite. The same is true for the ratios between *a3* and *a1* isoforms. We can see that CL1 has over 1000 times more *a4*/*a1* and *a3*/*a1* than LNCaP. In the PC3 cells the ratios of *a4*/*a1* and *a3*/*a1* are higher than LNCaP, but they are not as high as we were expecting. The levels of *a3* mRNA do not change significantly between LNCaP and CL1 but PC3 has 4 times more than the rest. These results suggest that the *a3* isoform increase seen in PC3 could be responsible for the speculated increase in vesicle recycling.

The use of immunocytochemistry allows us to visualize the location of the E subunit of the V-ATPase with a maximum resolution of 200nm. Since this technique cannot be used to quantify amounts of each protein we should only see a difference in spatial distribution of the proteins. Actin is a microfilament part of the cytoskeleton. It is present throughout the cell and should help us visualize the edges of the cell. We can see that staining for the V-ATPase shows accumulation at the cell surface of both CL1 and PC3 but not LNCaP. Overlay of the two staining helps visualize estimates of colocalization events but they neither reflect the three-

dimensional nature of the antigen nor the restrained resolution along the z-axis. Using a different confocal microscope (Nikon A1RMP) we could perform an intensity correlation coefficient-based (ICCB) analysis. This is a global statistic approach to visualize colocalization events regardless of the proportions of the molecules (61). This approach allows us to observe with more detail the colocalization of the two stains. LNCaP does not show many colocalization events while CL1 and PC3 do. Unfortunately, the limitations of microscopy can only allow us to conclude that the colocalization of the two proteins occurs when both are at least 200 nm apart. Actin is bound to proteins attached to the inner leaflet of the plasma membrane, within 200nm of actin there could be acidic vesicles that could show as colocalization events.

The V-ATPase has been shown to have a role in cancer multi drug resistance. Several chemotherapeutic drugs have a pK_a close to the physiological pH. By moving these drugs into acidic vesicles it is possible for the cell to inactivate the drug and extrude it through vesicle recycling. It is also possible that pmV-ATPases when acidifying the extracellular environment deactivate the drug before it enters the cell. Docetaxel is a commonly used chemotherapeutic drug in the treatment of several cancers including prostate cancer. By using a sub-lethal dose of bafilomycin in conjunction with docetaxel we can see a reduction in IC_{50} (concentration of drug required to kill 50% of the cells) for all the cell lines. LNCaP and CL1 both show a reduction in IC_{50} of 1 nM. It has been shown that prostate cancer treated androgen deprivation therapy exhibit not only resistance to the drug but also increased metastatic potential. Since the CL1 cell line was derived from LNCaP through androgen deprivation, it is possible that the cell line has become resistant to docetaxel. This is supported by the fact that the cytotoxicity performed on CL1 cell lines only kills a maximum of 45% of the cells even with the highest concentration of docetaxel. PC3 cells show a 300 nM change in the IC_{50} after the addition of bafilomycin. These results show not only that bafilomycin has a significant effect at increasing the cell's sensitivity to the drug but also that PC3 has an increased resistance compared to LNCaP. This resistance could be attributed to the increased expression of pmV-ATPase but

based on previous results this could be due to a decrease in the cell's ability to extrude the drug through vesicle recycling.

Based on these results we can conclude that there is an increased activity and expression of V-ATPase at the plasma membrane when comparing the most aggressive prostate cancer cell line with the non-metastatic one. The results from PC3 pointed at an involvement of V-ATPase in the metastatic phenotype but it was not always related to its presence at the plasma membrane.

BIBLIOGRAPHY

1. Huber, V.; De Milito, A.; Harguindery, S.; Reshkin, S. J.; Wahl, M.; Rauch, C.; Chiesi, A.; Pouyssegur, J.; Gatenby, R.; Rivoltini, L.; Fais, S. Proton dynamics in cancer. *J Transl Med* **2010,** *8,* 57.
2. Grinstein, S.; Rotin, D.; Mason, M. J. Na+/H+ exchange and growth factor-induced cytosolic pH changes. Role in cellular proliferation. *Biochim Biophys Acta* **1989,** *988,* 73-97.
3. Brianchini, L.; Kapus, A.; Lukacs, G.; Wasan, S.; Wakabayashi, S.; Pouyssegur, J.; Yu, F. H.; Orlowski, J.; Grinstein, S. Responsiveness of mutants of NHE1 isoform of Na+/H+ antiport to osmotic stress. *Am J Physiol 269,* C998-C1007.
4. Wang, J.; Singh, D.; Fliegel, L. The Na+/H+ exchanger potentiates growth and retinoic acid induced differentiation of P19 embryonal carcinoma cells. *J Biol Chem* **1997,** *272,* 26545-26549.
5. Noel, J.; Roux, D.; Pouyssegur, J. Differential localization of Na+/H+ exchanger isoforms (NHE1 and NHE3) in polarized epithelial cell lines. *J Cell Sci* **1996,** *109,* 929-939.
6. Rotin, D.; Steele-Norwood, D.; Grinstein, S. Requirement of the Na+/H+ exchanger for tumour growth. *Cancer Res* **1989,** *49,* 205-211.
7. Alper, S. L.; Chernova, M. N.; Stewart, A. K. Regulation of Na+ independent Cl/HCO3 exchangers by pH. *J. Pancreas* **2001,** *2,* 171-175.
8. Aronson, P. S.; Soleimani, M.; Grassl, S. M. Properties of the renal NA/HCO3 cotransporter. *Semin. Nephrol.* **1991,** *11,* 28-39.
9. Jiang, L.; Stuart-Tilley, A.; Parkash, J.; Alper, S. L. pHi and serum regulate AE2-mediated Cl/HCO3 exchange in CHOP cells of defined transient transfection status. *Am. J. Physiol* **1994,** *267,* C845-C856.
10. Linn, S. C.; Kudrycki, K. E.; Shull, G. E. The predicted translation product of a cardiac AE3 mRNA contains an N-terminus distinct from that of the brain AE3 Cl/HCO3 exchanger. *J. Biol. Chem.* **1992,** *267,* 7927-7935.
11. Soleimani, M.; Grassl, S. M.; Aronson, P. S. Stoichiometry of Na/HCO3 cotransport in basolateral membrane veiscles isolated from rabbit renal cortex. *J. Clin. Invest.* **1987,** *79,* 1276-1280.
12. Soleimani, M.; Lesoine, G. A.; Bergman, J. A.; Aronson, P. S. Cation specificity and modes of the Na/CO3:HCO3 cotransporter in renal basolateral membrane vesicles. *J. Biol. Chem.* **1991,** *266,* 8706-8710.
13. Karumanchi, S. A.; Jiang, L.; Knebelmann, B.; Stuart-Tilley, A. K.; Alper , S. L.; Sukhatme, V. P. VHl tumor suppressor regulates Cl-/HCO3- exchange and Na+/H+ exchange activities in renal carcinoma cells. *Physiol Genomics* **2001,** *5,* 119-128.

14. Poole, R.; Halestrap, A. Transport of lactate and other monocarboxylates across mammalian plasma membranes. *Am J Physiol* **1993,** *264 (4 Pt 1),* C761-C782.

15. Juel. Lactate-proton cotransport in skeletal muscle. *Physiol Rev* **1997,** *77,* 321-358.

16. Price, N. T.; Halestrap , A. P. The proton-linked monocarboxylate transporter (MCT) family: structure, function and regulation. *Biochem J* **1999,** *343,* 281-299.

17. Dimroth, P.; Wiedenmann, A.; Ballmoos, C. Essentials for ATP Synthesis by F1F0 ATP Synthases. *Annu Rev Biochem* **2009,** *78,* 649-672.

18. Duncan, T. M.; Bulygin, V. V.; Zhou, Y.; Hutcheon, M. L.; Cross, R. L. rotation of subunits during catalysis by Escherichia coli F1-ATPase. *Proc natl Acad Sci USA* **1995,** *92,* 10964-10968.

19. Sabbert, D.; Englebrecht, S.; Junge, W. Functional and idling rotatory motion within F1-ATPase. *Proc Natl Acad Sci USA* **1997,** *94,* 4401-4405.

20. Stock, D.; Leslie, A. G.; Walker , J. E. Molecular architecture of the rotary motor in ATP synthase. *Science* **1999,** *286,* 1700-1705.

21. Forgac, M. Vacuolar ATPases: rotary proton pumps in physiology and pathophysiology. *Nat Rev Mol Cell Biol* **2007,** *8,* 917-929.

22. Nishi, T.; Forgac, M. The vacuolar (H+)-ATPases: nature's most versatile proton pumps. *Nat Rev Mol Cell Biol* **2002,** *3,* 94-103.

23. Wilkens, S.; Forgac, M. Three-dimensional structure of the vacuolar ATPase proton channel by electron microscopy. *J Biol Chem* **2001,** *276,* 44064-44068.

24. Kawasaki-Nishi, S.; Nishi, T.; Forgac, M. Arg735 of the 100 kDa a subunit of the yeast V-ATPase is essential for proton translocation. *Proc Natl Acad Sci USA* **2001,** *98,* 12397-12402.

25. Bowman, E. J.; Bowman, B. J. V-ATPases as drug targets. *J Bioenerg Biomembr* **2005,** *37,* 431-435.

26. Pietrement, C. distinct expression patternt of different subunit isoforms of the V-ATPase in the rat epididymis. *Biol Reprod* **2006,** *74,* 185-194.

27. Toyomura, T.; Murata, Y.; Yamamoto, A.; Oka , T.; Sun-Wada, G. H.; Wada, Y.; Futai, M. From lysosomes to the plasma membrane: localizatio of vacuolar-type H+-ATPase with the a3 isoform during osteoclast differentiation. *J Biol Chem* **2003,** *278,* 22023-22030.

28. Hinton, A.; Sennoune, S. R.; Bond, S.; Fang, M.; Reuveni, M.; Sahagian, G. G.; Jay, D.; Martinez-Zaguilan, R.; Forgac, M. Function of a subunit isoforms of teh V-ATPase in pH Homeostasis and in vitro invasion of MDA-MB231 human breast cancer cells. *J Biol Chem* **2009,** *284,* 16400-16408.

29. Sennoun, S. R.; Bakunts, k.; Martinez, G. M.; Chua-Tuan, J. L.; Kebir, Y.; Attaya, M. N.; Martinez-Zaguilan, R. Vacuolar H+ ATPase in human breast cancer cells with distinct metastatic potential: distribution and functional activity. *Am J Physiol Cell Physiol* **2004,** *286,* 1443-1452.

30. Gocheva, V.; Joyce, J. A. Cysteine Cathepsins and the cutting edge of Cancer Invasion. *Cell Cycle* **2007,** *6,* 60-64.

31. Joyce, J. A.; Hanahan, D. Multiple Roles for cysteine Cathepsins in Cancer. *Cell Cycle* **2004,** *3,* 1516-1519.

32. Durand, R. E.; Olive, P. L. Resistance of tumor cells to chemo- and radiotherapy modulated by the three-dimensional architecture of solid tumors and spheroids. *Methods Cell Biol* **2001,** *64,* 211-233.

33. Ambudkar, S. B.; Dey, S.; Hrycyna, C. A.; Ramachandra, M.; Pastan, I.; Gottesman, M. M. Biochemical, cellular, and pharmacological aspects of the multidrug transporter. *Annu Rev Pharmacol Toxicol* **1999,** *39,* 361-398.

34. Gottesman, M. M.; Fojo, T.; Bates, S. E. Multidrug resistance in cancer: role of ATP-dependent transporters. *Nat Rev Mol Cell biol* **2002,** *2,* 48-58.

35. Martinez-Zaguilan, R.; Raghunand, N.; Lynch, R. M.; Bellamy, W.; Martinez, G. M.; Rojas, B.; Smith, D.; Dalton, W. S.; Gillies, R. J. pH and Drug Resistance. I. Functional expression of plasmalemmal V-type H-ATPase in Drug-resistant human breast carcinoma cell lines. *Biochem Pharmacol* **1999,** *57,* 1037-1046.

36. Raghunand, N.; Gillies, R. J. pH and drug resistance in tumors. *Drug Resist Updat* **2000,** *3,* 39-47.

37. Jemal, A.; Siegel, R.; Xu, J.; Ward, E. Cancer Statistics, 2010. *CA Cancer J Clin* **2010,** *60,* 277-300.

38. American Cancer Society. Cancer Facts & Figures 2010. *Atlanta: American Cancer Society* **2010,** 1-62.

39. National Cancer Institute. SEER Cancer Statistics Review, 1975-2007. **2009**.

40. Andreoiu, M.; Cheng, L. Multifocal prostate cancer: biologic, prognostic, and therapeutic implications. *Hum Pathol* **2010,** *41,* 781-793.

41. National Cancer Institute. Prostate Cancer Treatment (PDQ®), 2010. National Cancer Institute. http://www.cancer.gov/cancertopics/pdq/treatment/prostate/Patient/page4 (accessed Oct 19, 2010).

42. Chang, S. S. Treatment options for hormone-refractory prostate cancer. *Rev Urol* **2007,** *9,* S13-S18.

43. Niu, Y.; Chang, T. M.; Yeh, S.; Ma, W. L.; Wang, Y. Z.; Chang, C. Differential androgen receptor signals in different cells explain why androgen-deprivation therapy of prostate cancer fails. *Oncogene* **2010,** *29,* 3593-3604.

44. Petrylak, D. P.; Tangen, C. M.; Hussain, M. H. A.; Lara, P. N.; Jones, J. A.; Taplin, M. E.; Burch, P. A.; Berry, D.; Moinpour, C.; Kohli, M.; Benson, M. C.; Small, E. J.; Raghavan, D.; Crawford, E. D. Docetaxel and Estramustine Compared with Mitoxantrone and Prednisone for Advanced refractory Prostate Cancer. *N Engl J Med* **2004,** *351,* 1513-1520.

45. Berthold, D. R.; Pond, G. R.; Soban, F.; de Wit, R.; Eisenberger, M.; Tannock, I. F. Docetaxel plus prednisone or mitoxantrone plus prednisone for advanced prostate cancer: updated survival in the TAX 327 study. *J Clin Oncol* **2008,** *26,* 242-245.

46. Baker, S. D.; Sparreboom, A.; Verweij, J. Clinical Pharmacokinetics of Docetaxel. *Clin Pharmacokinet* **2006,** *45,* 235-252.

47. Snyder, J. P.; Nettles, J. H.; Cornett, B.; Downing, K. H.; Nogales , E. The binding conformation of Taxol in beta-tubulin: A model based on electron crystallographic density. *Proc Natl Acad Sci USA* **2001,** *98,* 5312-5316.

48. Sobel, R. E.; Sadar, M. D. Cell lines used in prostate cancer research: a compendium of old and new lines - part 1. *J Urol* **2005,** *173,* 342-359.

49. ATCC. Cell Lines and Hybridomas. http://www.atcc.org/ATCCAdvancedCatalogSearch/ProductDetails/tabid/452/Default.aspx?ATCCNum=CRL-1435&Template=cellBiology (accessed Oct 17, 2010).

50. Tso, C.; McBride, W.; Sun, J.; Patel, B.; Tsui, K.; Paik, S. H.; Gitlitz, B.; Caliliw, R.; Ophoven, A. V.; Wu, L.; deKernion, J.; Belledegrun, A. Androgen Deprivation induces selective outgrowth of aggressive hormone-regractory prostate cancer clones expressing distinc cellular and molecular properties not present in parental androgen-dependent cancer cells. *Cancer J* **2000,** *6,* 220-233.

51. Martinez-Zaguilan, R.; Martinez , G. M.; Lattanzio, F.; Gilles, R. Simultaneous measurement of intracellular pH and Ca using the fluorescence of SNARF-1 and fura-1. *Am J Physiol* **1991,** *363,* C297-C309.

52. Roos, A.; Boron, W. F. Intracellular pH. *Physiol Rev* **1981,** *61,* 296-434.

53. Martinez-Zaguilan, R.; Lynch, R. M.; Martinez, G. M.; Gillies, R. J. Vacuolar-type H-ATPases are functionally expressed in plasma membranes of human tumor cells. *Am J Physiol* **1993,** *363,* C1015-C1029.

54. Fletcher, P. A.; Scriven, D. R.; Schulson, M. N.; Moore, E. D. Multi-Image colocalization and its statistical significance. *Biophys J* **2010,** *99,* 1996-2005.

55. Lowry, O. H.; Rosebrough, N. J.; Farr, A.; Randall, R. Protein measurement with the folin phenol reagent. *J. Biol Chem* **1951,** *193,* 265-275.

56. Chifflet, S.; Torriglia, A.; Chiesa, R.; Tolosa, S. A Method for the Determination of Inorganic Phosphate in the Presence of Labile Organic Phosphate and High concentration sof Protein: Application to Lens ATPases. *Anal Biochem* **1988,** *168,* 1-4.

57. Gonzalez-Romo, P.; Sanchez-Nieto, S.; Gavilanes-Ruiz, M. A modified colorimetric method for the determination of orthophosphate in the presence of high ATP concentrations. *Anal Biochem* **1992,** *200,* 235-238.

58. Woodson, S. A.; Leontis, N. B. Structure and dynamics of ribosomal RNA. *Current Opinion in Structural Biology* **1998,** *8,* 294-300.

59. McDonough, A. A.; Zhang, Y.; Shin, V.; Frank, J. S. Subcellular distribution of sodium pump isoform subunits in mammalian cardiac myocytes. *Am J Physiol* **1996,** *270,* C1221-C1227.

60. Yakuvchuk, P.; Ekaterina, P.; Frank-Kamenetskii, M. D. Base-stacking and base-pairing contributions into thermal stability of the DNA double helix. *Nucleic Acids research* **2006,** *34,* 564-574.

61. Bolte, S.; Cordelieres, F. P. A guided tour into subcellular colocalization analysis in light microscopy. *J Microsc* **2006,** *224,* 213-232.

62. Swaminathan, R.; Bickness, S.; Periasamy, N.; Verkman, A. S. Cytoplasmic viscosity near the cell plasma membrane: translational diffusion of a small fluorescent solute measured by total internal reflection-fluorescence photobleaching recovery. *Biophys J* **1996,** *71,* 1140-1151.

63. Sanchez-Armass, S.; Sennoune, S.; Maiti, D.; Ortega, F.; Martinez-Zaguilan, R. Spectral Imaging Microscopy demonstrates cytoplasmic pH oscillations in Glial cells. *Am J Physiol Cell Physiol* **2005,** *290,* C524-C538.

64. Cammann, K. Ion-selective bulk membranes as models. *Top Curr Chem* **1985,** *128,* 219-258.

65. Amar-Costesec, A.; Wibo, M.; Thines-Sempoux, D.; Beaufay, H.; Berthet, J. Analytical study of microsomes and isolated subcellular membranes from rat liver. *J Cell Biol* **1974,** *62,* 717-745.